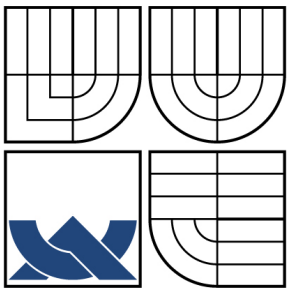

VYSOKÉ UČENÍ TECHNICKÉ V BRNĚ

BRNO UNIVERSITY OF TECHNOLOGY

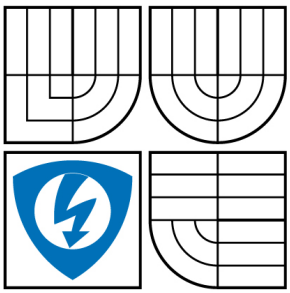

FAKULTA ELEKTROTECHNIKY A KOMUNIKAČNÍCH TECHNOLOGIÍ

ÚSTAV ELEKTROTECHNOLOGIE

FACULTY OF ELECTRICAL ENGINEERING AND COMMUNICATION

DEPARTMENT OF ELECTRICAL AND ELECTRONIC TECHNOLOGY

STUDY OF THE PROPERTIES OF HYPERPOLARIZED XENON-129 FOR MAGNETIC RESONANCE IMAGING

STUDIUM VLASTNOSTÍ HYPERPOLARIZOVANÉHO XENONU-129 PRO ZOBRAZOVÁNÍ MAGNETICKOU REZONANCÍ

DIZERTAČNÍ PRÁCE

DOCTORAL THESIS

AUTOR PRÁCE — Ing. JAN RYCHNOVSKÝ

AUTHOR

VEDOUCÍ PRÁCE — prof. Ing. KAREL BARTUŠEK, DrSc.

SUPERVISOR

BRNO 2009

This doctoral thesis was composed in the

Institute of Scientific Instruments

AS CR, v. v. i.,

accredited for doctoral study degree

“Microelectronics and technology”

by a certificate from MEYS issued on

13.3.2003

under the supervision of

prof. Ing. Karel Bartušek, DrSc.

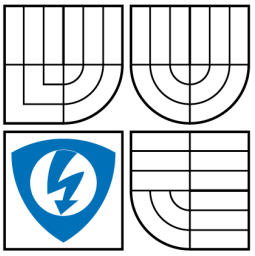

VYSOKÉ UČENÍ TECHNICKÉ V BRNĚ

Fakulta elektrotechniky a komunikačních technologií

Ústav elektrotechnologie

Dizertační práce

doktorský studijní obor

Mikroelektronika a technologie

Student:	Ing. Jan Rychnovský	***ID:***	16553
Ročník:	1	***Akademický rok:***	2008/2009

NÁZEV TÉMATU:

Studium vlastností hyperpolarizovaného xenonu-129 pro zobrazování magnetickou rezonancí

POKYNY PRO VYPRACOVÁNÍ:

DOPORUČENÁ LITERATURA:

Termín zadání: ***Termín odevzdání:***

Vedoucí práce: prof. Ing. Karel Bartušek, DrSc.

prof. RNDr. Vladimír Aubrecht, CSc.
Předseda oborové rady

UPOZORNĚNÍ:

Statement

I declare that I have worked on this thesis independently, under the guidance of my supervisor, using only listed references.

Brno, 24th August, 2009 Ing. Jan Rychnovský

Acknowledgements

I would like to thank my colleagues for their help and support during my work on the thesis.

First and foremost I would like to thank prof. Karel Bartušek for his exceptional help and guidance.

My deep appreciation goes to Dr. Zenon Starčuk, Jr. for his help and suggestions during the experimental part of my research and for helping me with the mathematical and physical background to my thesis. My thanks also goes to Dr. Zdeněk Buchta for an exceptional co-operation during my research of optical part of the xenon hyperpolarization device.

I would also like to thank to Mr. Richard Vašíček and Mr. Stanislav Šlechtický for their precise work with and on the glass parts and to Mrs. Tatiana Šarlejová for her precise work on the vacuum parts and her help with preparing of some experiments.

Least but not last, I would like to thank my parents and Lucie for their endless support, love and encouragement.

Keywords

hyperpolarization, ^{129}Xe, relaxation time, nuclear magnetic resonance, laser diode, optical pumping, spin exchange, rubidium

Klíčová slova

hyperpolarizace, ^{129}Xe, relaxační čas, jaderná magnetická resonance, laserová dioda, optické čerpání, spinová výměna, rubidium

Abstract

The production of hyperpolarized gases (HpG), predominantly helium (^{3}He) or xenon (^{129}Xe), have found a steadily increasing range of applications in magnetic resonance imaging (MRI). Neither helium nor xenon are normally present in the body, thus the magnetic resonance experiments do not suffer from unwanted background signals. It has been demonstrated by several techniques of hyperpolarization that the magnetic polarization (magnetization) of the noble gas nuclei can be increased to levels that make practical application feasible. Hence, hyperpolarized gases may become a useful tool for non-invasive investigation of human lung ventilation, permitting static imaging during breathhold or probing the dynamics of inhalation/exhalation, or functional imaging. In inanimate nature, hyperpolarized gas can be used as a contrast medium for microporous materials, such zeolites, constructive materials in civil engineering, etc.

This thesis describes the development and construction of a xenon (^{129}Xe) hyperpolarization (Hp) device. Buying hyperpolarized xenon from other research centres abroad is inefficient mainly because HpXe transportation must be performed fast and under specific conditions. That was the main motivation for developing our own technology for production of HpXe. Well-handled technology could allow a medical cooperation or cooperation with teams dealing with in/animate nature (microporous material, gels, agriculture, animals, etc.).

The main aim of this work is to study the hyperpolarized noble gases theory with concern to ^{129}Xe and to experimentally prove and measure xenon relaxation times by the NMR. Since it is possible to store hyperpolarized noble gases for later use, this doctoral thesis also explores the potentials of hyperpolarized noble gas storage system and its theoretical and experimental solution.

Mainly two types of experiments are described in this thesis. In both experiments, sealed cylindrical Simax sample filled with xenon and supplement gas – nitrogen, helium were used. The first type of experiment is based on thermally polarized xenon and the second on hyperpolarized xenon. For hyperpolarization of ^{129}Xe a high-power laser was used. In this experiment, the relation between power spectral density of optical pumping beam and efficiency of HpXe production process was investigated. The optimal duration of optical pumping and relaxation times of HpXe were investigated too.

Abstrakt

Produkce hyperpolarizovaných plynů, především helia (^{3}He) nebo xenonu (^{129}Xe), nachází stále rostoucí rozsah aplikací v zobrazování magnetickou rezonancí (MRI). Helium ani xenon nejsou obyčejně obsaženy v těle a experimenty tedy nejsou ovlivněny nechtěným signálem z okolních tkání. Ukázalo se, že několika hyperpolarizačními technikami může být magnetická polarizace (magnetizace) jader vzácných plynů zvýšena na hladinu, se kterou jsou praktické aplikace proveditelné. Hyperpolarizované plyny mohou tedy být užitečným nástrojem pro neinvazivní zkoumání lidského dýchání, dovolující statické zobrazování během zadržení dechu nebo zkoumání dynamiky výdechu nebo nádechu, nebo funkčního zobrazování. V neživé přírodě, mohou být hyperpolarizovaný plyny využity jako kontrastní látka při studiu mikroporézních materiálů, jako jsou zeolity, stavební látky a hmoty, atd.

V této doktorské práci je popsán vývoj a konstrukce aparatury pro hyperpolarizaci xenonu (izotopu ^{129}Xe). Nákup hyperpolarizovaného xenonu od jiných výzkumných center v zahraničí a jeho dovážení by ovšem nebylo efektivní a to zejména z důvodu náročnosti zajištění potřebných fyzikálních podmínek pro přepravu hyperpolarizovaného plynu. Toto bylo hlavní motivací k vývoji vlastní technologie pro přípravu hyperpolarizovaného xenonu. Se zvládnutou technologií by bylo možné navázat spolupráci s medicínskými zařízeními, nebo s týmy zabývající se živou nebo neživou přírodou (např. při studiu mikroporézních materiálů, gelů, v zemědělských aplikacích nebo při výzkumu využívajících zvířat, atd.).

Cílem této práce je studium teorie hyperpolarizovaných vzácných plynů se zaměřením na ^{129}Xe a experimentální ověření a změření relaxačních časů pomocí jaderné magnetické rezonance. Vzhledem k tomu, že je možné hyperpolarizované vzácné plyny skladovat pro pozdější využití, se tato práce také zabývá možnostmi zásobníku hyperpolarizovaného vzácného plynu a jeho teoretickým a experimentálním řešením.

V této práci jsou popsány především dva základní typy experimentů přípravy hyperpolarizovaného xenonu. V obou jsou využity zatavené válcové skleněné vzorky naplněné xenonem a doplňujícím plynem – dusíkem, heliem. První z experimentů se zabývá měřením vlastností termálně polarizovaného xenonu a druhý měřením vlastností hyperpolarizovaného xenonu. Pro hyperpolarizaci ^{129}Xe bylo použito výkonového laseru a experimentálně byla zkoumána jednak míra polarizace na základě změny spektrální hustoty čerpacího laserového svazku a dále pak optimální doba optického čerpání ^{129}Xe a relaxační časy xenonu.

Content

1. Introduction

In the 1950s Alfred Kastler developed an Optical Pumping (OP) technique that earned him the Nobel Prize for Physics in 1966 [1]. Optical pumping is defined as a process in which light is used to excite electrons from a lower energy level in an atom or a molecule to a higher one. This process is commonly used in laser construction to pump the active laser medium so as to achieve population inversion [2].

Thereafter, it was observed [3] that when buffer gases are used in the alkali OP experiments, the nuclear spin polarization of the noble-gases is enhanced. By using OP of alkali metal atoms and atomic spin-exchange collisions [4, 5], as published in the early 1970s, huge enhancement of magnetic polarization of atom nuclei can be achieved [6-15]. The polarization achieved by this technique exceeds the normally utilized thermal equilibrium level produced in the magnets of standard nuclear magnetic resonance (NMR) systems by 4 to 5 orders of magnitude. Therefore, despite the low spin density characteristic for the gaseous state, hyperpolarized gases (HpG) can be used as sources of NMR signals detectable with good signal-to-noise ratios (SNR), which are comparable to or higher than those of water protons and independent of the static magnetic field strength.

These signals are endowed with many interesting properties. For instance, HpG may indicate the presence of oxygen due to the polarization sensitivity to the presence of paramagnetic substances. Further properties of xenon – its high electronic polarizability, hydrophobic nature and solubility in lipids [16] – enable the xenon atoms to bind to other chemicals and reflect them by changes of the resonance frequency, to dissolve in liquids, to cross biological barriers etc. These properties have formed the basis on which a variety of HpG applications have appeared during last 10-15 years in a wide range of NMR disciplines, mainly in medicine, biology, material sciences and chemistry.

1.1. State of the art

At present time, medical applications of HpG especially are considered an attractive concept [17, 18]. Neither helium nor xenon are normally present in the body, so the magnetic resonance (MR) experiments do not suffer from unwanted background signals. Among the potential medical applications, the opportunity to image organs with low water content and/or with air spaces, such as colon or lungs, has raised considerable amount of interest. Current conventional imaging techniques cannot provide good images of these hollow spaces as well as the surrounding tissue. The described applications show that HpG may become a useful tool for non-invasive investigation of human lung ventilation, permitting static imaging during breathhold, imaging of the dynamics of inspiration/expiration or functional imaging. Lung physiology and function in healthy or diseased state can be thus more accurately evaluated and assessed if a suitable multinuclear NMR system is available.

So far, hyperpolarized (Hp) helium-3 (^{3}He) has proven to have the greatest potential for the elucidation of physiological and pathophysiological processes, detecting small changes in the distribution of ventilation within the peripheral bronchial system, assessment of diffusivity of ^{3}He atoms within the airways and the acinar regions, as well as quantification of diffusion coefficients to characterize the distribution of the alveolar size. Due to the state of environmental factors, industrial influences, increasingly aged population, and smoking habits, use of hyperpolarized helium for studies of chronic obstructive pulmonary diseases (COPD) is of growing importance. Unlike the insensitive conventional tests, magnetic resonance imaging (MRI) using hyperpolarized ^{3}He can serve as a non-invasive technique for early diagnosis, differentiation, and staging of COPD.

However, the use of ^{3}He is not without problems. It is extracted from expired tritium drained out of hydrogen bombs and so the ^{3}He supply is limited and its price is high (about 1000 Euro/litre, purity 99.91%). In contrast to helium, ^{129}Xe is abundant and cheaper (about 14-15 Euro/litre for xenon with natural isotopic concentrations, with 26% of ^{129}Xe). For comparison, isotopically enriched ^{129}Xe (89-91%) costs about 220 Euro/litre and isotopic pure ^{129}Xe (99.8%) costs about 2 290 Euro/litre. The prices are based on April 2009 data provided by supplier firms, such as Linde, Chemgas, Eurisotop and AirProducts.

Some experimental values of hyperpolarized ^{129}Xe were measured. The new method to image pulmonary perfusion and gas exchange by intravenous injection of hyperpolarized ^{129}Xe dissolved in saline was presented by [19]. The T_1 relaxation time of ^{129}Xe in the shaker with saline was ~12 min in 2 T system.

Like ^{3}He, ^{129}Xe experiences long relaxation times in matter of hours. The Xe molecular formation rate at 1 atm is about $4 \cdot 10^7 s^{-1}$. That gives us an estimated T_1 for gaseous ^{129}Xe of around 3 hours, which is about what is observed in [20]. Solid phase ^{129}Xe relaxation can be very long, 2.4 hours at 77K and 100's of hours at 4.2 K [21]. [22].

In blood HpXe T_1 relaxation time of only 4.5 s was observed [23], which was caused by HpXe strong interaction with environment (e.g. lipids), enhancing T_1 and reducing signal. The next presented result introduces T_1 relaxation times for deoxygenated and oxygenated pure perfluorooctyl bromide to be 312 ± 25 s and 90 ± 31 s respectively. The T_1 relaxation times for deoxygenated and oxygenated distilled water were found to be 137 ± 6 s for deoxygenated and 95 ± 10 s for oxygentaed. The measuring was obtained in 1.89 T MR system.

The T_1 in brain tissue was measured to be 13.95 ± 1.23 s in 2.35 T [24].

In [25] is described the experiment concerning T_1 of the xenon in rat's brain. The T_1 relaxation time has been measured in vitro to fluctuates from 18 s in oxygenated brain tissue to 22 s in deoxygenated brain tissue. The experiments were performed using a 4.7 T spectrometer.

T_1 relaxation times give in [13] and measured directly in the cell for optical pumping are given, during the hyperpolarization of Xe by Ti:Sa laser, in tens of seconds, based on the temperature and the pressure of Xe and the pressure of N_2 cca 200mbar. T_1 relaxation time in a 3 T tomograph is assessed in the order of minutes.

It is necessary to say that the published results of measured relaxation times from different research groups vary depending on the type of experiment, used chemicals and

a quality of the used experimental device. It is not possible to give all the results and configurations.

Xenon diffuses less rapidly than helium, which should ultimately yield sharper MR images. However, because of the lower magnetogyric ratio (2.75 times), experiments with ^{129}Xe are less sensitive than those with ^{3}He. Furthermore, xenon is harder to hyperpolarize and store than helium. Some specific problems arise from the fact that xenon, unlike helium, dissolves quite well in blood and despite its classification as an inert gas it interacts with many biological chemicals. Xenon passes very well across the blood-brain barrier and produces anesthesia and euphoria (the mechanism of these effects is not yet understood), which may result in some complications during clinical investigations. However, despite these problems, it is anticipated that xenon imaging of the lungs could be brought to the same level of quality as that of helium imaging. Some physical properties of noble gases ^{129}Xe and ^{3}He are shown in Tab.1.

Tab. 1: *Important physical properties of ^{129}Xe and ^{3}He. Adapted and modified from [43].*

Parameter	^{129}Xe	^{3}He
Nuclear spin, K [ħ]	½	½
Natural abundance [%]	26.4	$1.37 \cdot 10^{-4}$
Gyromagnetic ratio, γ [MHz/T]	11.777	32.434
Normalized gyromag. ratio, γ/γ_H	0.276	0.762
T_1 relaxation time limit [hours/atm]	4.1	744
Chemical shift range	7500	0.8
Optical pumping duration [min]	5	>120

It appears that by exploiting the same properties, numerous extensions of the medical application of xenon are possible beyond lung space imaging [26-37]. Many of the NMR parameters of xenon, including its resonance frequency and relaxation rates, strongly depend on the nature of its physiochemical surroundings. It has been found that xenon may also prove itself useful in the studies of the brain and for tracing blood flow for applications such as perfusion imaging and angiography, as well as functional brain imaging. In these applications, instead of inhalation, the hyperpolarized xenon can be delivered into the tissues by local injections of biologically compatible solutions of carriers in which the required magnitudes of xenon concentration and polarization lifetime can be achieved. For in vivo studies, the injection can be administered intravenously, intra-arterially, or directly into the target organ, depending on the application and regarding the extent of invasiveness. Ultimately, the future utility of hyperpolarized xenon for improving sensitivity and contrast in clinical or medical science applications will depend on whether it actually improves upon present methodologies. Certainly, there are still areas that require an intensive research and methodological work as well, since the research is far from finished.

Besides the biomedical applications, hyperpolarized xenon (HpXe) can be used with advantage to improve studies of the molecular structure and dynamics in such systems as zeolites, catalysts, semiconductors, nanocrystals, liquid crystals, polymers or proteins [30-37].

In solutions, HpXe may be of special importance for the different type of molecular interaction investigation as well as for the selective detection and probing of chemical and structural environment of the xenon binding sites in biomacromolecules.

HpXe can be also used for studies of different solid surfaces and interfaces (through, for instance, spin polarization-induced nuclear Overhauser effect, SPINOE). The possibility of all these applications is due to the fact that the xenon atom (in contrast to helium) possesses a polarizable electron cloud which leads to its strong interactions with molecules and materials and which may result in very large chemical shifts in the observed xenon NMR spectra.

Furthermore, hyperpolarized noble gases open an exciting new frontier to "zero-field NMR". Expensive magnets representing centrepieces of MRI systems can be replaced by inexpensive low field magnets in imaging experiments based on the use of HpG. It is thanks to greater occupation of energy levels by the optical pumping than by greater base magnetic field. The effect is more described in Chapter 4. Another approach that could further improve the sensitivity of such low field MRI systems is based on using a superconducting quantum interference device (SQUID) to detect the NMR signal of the HpG [13].

Two methods of achieving the hyperpolarization of noble gases are known: a direct metastability exchange applicable to ^{3}He only, and indirect spin-exchange method involving polarization of atoms of alkali metal (Rb) vapours followed by polarization transfer to noble gas atom nuclei through spin-exchange collisions (Fig. 1).

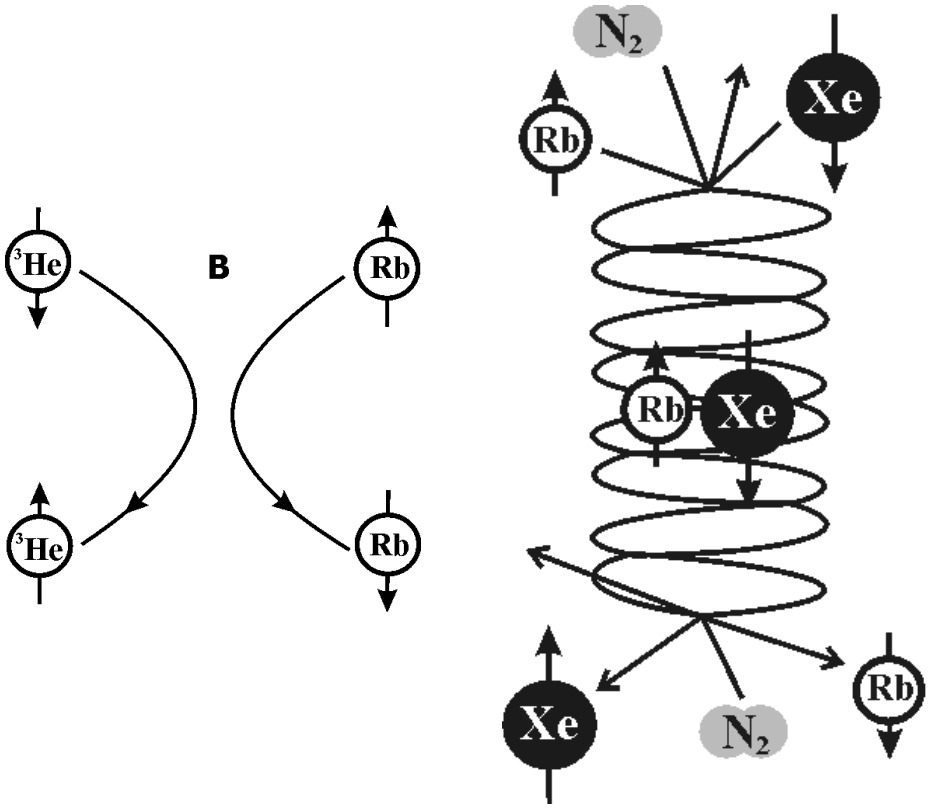

Fig. 1: *Spin-exchange process with 3He is performed by binary collisions (left hand side). Spin-exchange process with 129Xe is performed by the formation of van der Waals molecules (right hand side).*

The latter method is applicable to both ^{3}He and ^{129}Xe. The most serious problem of these procedures is the long-term preservation of the unequilibrium polarization, which is adversely affected by all T_1 relaxation mechanisms that disrupt the adiabaticity of the polarization evolution – spin-rotation interaction between HpG nuclear spins, dipolar interaction of HpG nuclear spins with paramagnetic molecules, spin motion in inhomogeneous fields, and especially collisions with the container walls. Under favorable conditions, T_1 relaxation times of several days for ^{3}He and several hours for ^{129}Xe have been observed (extensible to several days by preservation at liquid helium temperature), as shown in Tab.1 As the conditions after HpG has been administered for NMR, measurements are necessarily much less favorable, the relaxation time is considerably reduced to several seconds. Effective transverse relaxation times T_2^* of about 10 ms have been observed with ^{3}He, and 20-40 ms in ^{129}Xe. As the loss of polarization, due to T_1 and T_2 relaxation times, is irrecoverable, these facts impose certain requirements for the choice and setup of NMR methods. For imaging, methods known as low-flip-angle methods (such as FLASH) and/or multiple-echo methods (such as EPI or FSE) can be used. The large ^{129}Xe spectral bandwidth of >250 ppm has to be taken into account in both spectroscopy and imaging as it implicates the minimum sampling rates and together with the maximum achievable magnetic field gradient strength it determines the chemical-shift displacement image artefacts. Because of the considerable number of parameters affecting the final image or spectrum quality, it can hardly be expected that the protocols used so far could be optimal.

Currently, about a dozen of laboratories in the world is known to deal with laser-polarization of noble gases, including those of Princeton Univ. (Princeton, NJ), Univ. of California (Berkeley Lab., Berkeley, CA), Harvard University (Walsworth Group, Boston, MA), École normale supérieure (Lab. Kastler Brossel, Paris), Univ. of Virginia (Charlotteville, VA), Royal Marsden NHS Trust (London, UK), Univ. J. Fourier (INSERM, Grenoble), Carleton Univ. (Herzberg Lab., Ottawa, ON), Mainz Univ. (Inst. für Physik, Mainz), Phys.-Tech. Bundesanstalt (Biomedical Optics, Berlin), Michigan Univ. (Dept. of Physics, Ann Arbor, MI), NIST (Physics Lab., Gaithersburg, MD), Univ. of Nottingham (School of Phys. & Astr., Nottingham, UK), Univ. of Utah (Salt Lake City, UT), Univ. Compl. de Madrid (Spain), Jagellonian Univ. (Krakow, Poland), etc.

In many of these universities, this research accompanies more fundamental physical research (such as light storage, Bose-Einstein condensate) using similar technology.

The significance of such a co-operation may be justified by the search for cost-efficient means of HpG production for medical users and/or for low-field scanners, e.g. for lung examination or angiography. The real needs will depend on whether magnetic resonance imaging (MRI) with HpG gets approved for clinical diagnostics of at least lung diseases. Non-medical applications, especially those related to studies of various biomolecules [30-33] and porous materials [34-38] might also gain an increased interest.

A state-of-the-art ^{3}He polarizer running in the metastability exchange regime was developed at the University of Mainz [39, 40] and it is used in collaborations for MRI experiments using hyperpolarized ^{3}He. The polarizer can produce up to 1 liter/hour of 50% polarized ^{3}He and higher polarization can be obtained for lower flow rates. Recently a more compact and less-expensive design was demonstrated at NIST [41] being able to generate 1 liter/hour of 15% polarized helium.

Since the 1970s scientific circles have displayed an increasing interest in hyperpolarized noble gases. Our desire to use hyperpolarized noble gases in material investigation and biomedical application led us to think about a possible development of our own technology for noble gases hyperpolarization. When we take into consideration the cost of hyperpolarized noble gases production, its transportation, and the storage complications, it is more convenient to develop one's own hyperpolarization technique. Another reason for developing one's own hyperpolarization technique is the difficulty connected with a full take over of the hyperpolarization technique used in other laboratories concerned with the issue.

In the ISI AS CR, v.v.i. the properties of ^{129}Xe have been measured in sealed glass cell. The sample consisted of 100 kPa of xenon, 200 kPa of nitrogen, and a small piece of rubidium. The hyperpolarized xenon spectral line amplitude was enhanced about 100 times than the one of thermally polarized xenon spectral line. The relaxation time T_1 was between 360 and 549 ms [42].

2. Aims of the doctoral thesis

The main aim of the doctoral thesis is to generate a hyperpolarized ^{129}Xe and investigate its relaxation characteristics. This fact led to several series of experiments and result evaluations.

Because of the possibility to store hyperpolarized noble gases for later use, this doctoral thesis also explores the potential of hyperpolarized noble gas storage system and its theoretical and experimental solution.

3. Structure of the doctoral thesis

The doctoral thesis deals with the design and construction of a compact system designed for optical pumping of ^{129}Xe, which is one of natural xenon gas isotopes. Because of suggested system complexity and extensiveness, which connects and takes advantage of knowledge of vacuum techniques, coherent optics, and NMR branches, the work on this thesis was divided into several parts and phases.

The motivation and reasons for the construction of the system for xenon hyperpolarization are explained in the Introduction. There, I slightly touch upon the theory background, which is more described in chapter four.

In chapter two, the two main aims of the thesis are formulated and in chapter three, the structure of the thesis is described.

Chapter 4 includes essential theory related to this work. It explains base of the NMR, NMR techniques and NMR technique which was used for my experiments. In the subchapter (4.1.) the theory about nuclear spin is mentioned, in (4.2.) the nuclear polarization and in (4.3.) the hyperpolarization techniques are mentioned. The last subchapter is dedicated to used NMR technique for conducted experiments.

In chapter 5, there are described three, independently functioned, main parts of an experimental device. The first described part is a vacuum system (5.1.). The subchapters of Chapter 5.1 provide more detailed description of individual vacuum parts. Subchapters 5.2 and 5.3 deal with the optical (5.2) and NMR (5.3.) parts of the experimental device.

Chapter 6 describes experimental results with 129Xe. First, the results concerning thermally polarized xenon are described (6.1.). Second, the results of hyperpolarized ^{129}Xe experiments are mentioned (6.2.) and compared to results of experiments with thermally polarized xenon. The hyperpolarization experiments were conducted by free running and ECL laser diode for rubidium optical pumping, and the results were compared. All these experiments were accomplished with sealed glass cell. The subchapter 6.3. includes information about optical pumping under continual flow and describes the experimental arrangement. The last subchapter 6.4. discusses the impact of a glass material on T1 relaxation time.

Last Chapter Conclusion reviews results and experimental arrangements for xenon hyperpolarization. New ideas and procedure improvements in techniques of xenon hyperpolarization are suggested.

4. Hyperpolarized noble-gases and NMR

The production of hyperpolarized gases, predominantly helium (^{3}He) or xenon (^{129}Xe), have found a steadily increasing range of applications in magnetic resonance imaging (MRI). It has been demonstrated that by several techniques of hyperpolarization, the magnetic polarization (magnetization) of the noble gas nuclei can be increased to levels that make practical application feasible. Hence, hyperpolarized gases may become a useful tool for non-invasive investigation of biomedicine applications and materials too.

In order to narrow down the very complex theory, this chapter was constructed based on the following literature [43, 44, 45, and 46].

4.1. The nuclear spin

A fundamental property of the atomic nucleus is the nuclear spin, described by the spin quantum number I. Strictly speaking, the nuclear spin is a purely quantum mechanical quantity, but in terms of classical physics it may be viewed as an angular momentum - the nucleus rotates around its axis. Many atomic nuclei (mainly those with an odd mass number) have a nonzero spin quantum number and can be studied with NMR, e.g., ^{1}H, ^{3}He, ^{13}C, ^{15}N, ^{31}P and ^{129}Xe, etc. Nuclei having the spin quantum number I = 0 "do not rotate" and cannot be studied with NMR. Most nuclei with an even mass number, e.g., ^{4}He and ^{12}C belong to this latter group. Due to its positive charge, a rotating nucleus constitutes of a microscopic ring current, giving rise to a microscopic magnetic moment $\boldsymbol{\mu}$, which can be pictured as a microscopic compass needle. When placed in an external magnetic field $\boldsymbol{B}_0$, the magnetic moments orient themselves along the magnetic field; but as opposed to compass needles, only discrete orientations are allowed. The number of allowed orientations is given by $2I+1$, and each orientation is associated with a distinct quantum energy E_m:

$$E_m = -\boldsymbol{\mu} \cdot \mathbf{B}_0 = m\gamma\hbar B_0 \tag{1}$$

where $m = -I, -I+1, \ldots, +I$ is the magnetic quantum number, and the constant γ is called the gyromagnetic ratio, characteristic of each atomic nucleus. The magnetic moment $\boldsymbol{\mu}$ cannot be oriented parallel to $\boldsymbol{B}_0$, and will thus experience a torque trying to align $\boldsymbol{\mu}$ with $\mathbf{B}_0$. In analogy with a top rotating in the earth's gravity field, this torque will cause $\boldsymbol{\mu}$ to revolve around $\boldsymbol{B}_0$ with an angular frequency ω, denoted the Larmor frequency:

$$\omega = \gamma B_0 . \tag{2}$$

The nucleus investigated in this thesis ^{129}Xe have the spin quantum number $I = \frac{1}{2}$, and thus two orientations are possible: namely, parallel to $\boldsymbol{B}_0$ ("spin up", $\uparrow$) and anti-parallel to $\boldsymbol{B}_0$ ("spin down", $\downarrow$). By vector addition of all the magnetic moments,

oriented in either the "up" or the "down" direction, a macroscopic magnetization vector parallel to $\boldsymbol{B}_0$ is obtained:

$$\mathbf{M} = \sum \boldsymbol{\mu}_{\uparrow} + \sum \boldsymbol{\mu}_{\downarrow} . \tag{3}$$

However, this magnetization cannot be observed unless a rotating, transverse component is created. Such a component is created by tilting, or "flipping", $\boldsymbol{M}$ sideways, which in turn is accomplished by applying a second magnetic field, $\boldsymbol{B}_1$, perpendicular to $\boldsymbol{B}_0$, and oscillating with the Larmor frequency. The angle at which the $\boldsymbol{B}_1$ field tilts $\boldsymbol{M}$ is called the "flip angle". When a sample is placed near or inside a receiver coil in the magnetic field, the transverse magnetization component (rotating with Larmor frequency) will induce a voltage across the terminals of the receiver coil with amplitude proportional to the magnitude of $\boldsymbol{M}$.

4.2. Nuclear polarization

The number of nuclei populating each energy state may be denoted $N_{\uparrow}$ and $N_{\downarrow}$, respectively. If the two populations are equal, their magnetic moments cancel, resulting in zero macroscopic magnetization, and thus no NMR signal. Due to the slightly higher energy associated with the "down" direction, the number of nuclei pointing "down" will, however, be slightly fewer than the number of nuclei pointing "up" $\left(N_{\downarrow} < N_{\uparrow}\right)$ under thermal equilibrium conditions (Fig 2).

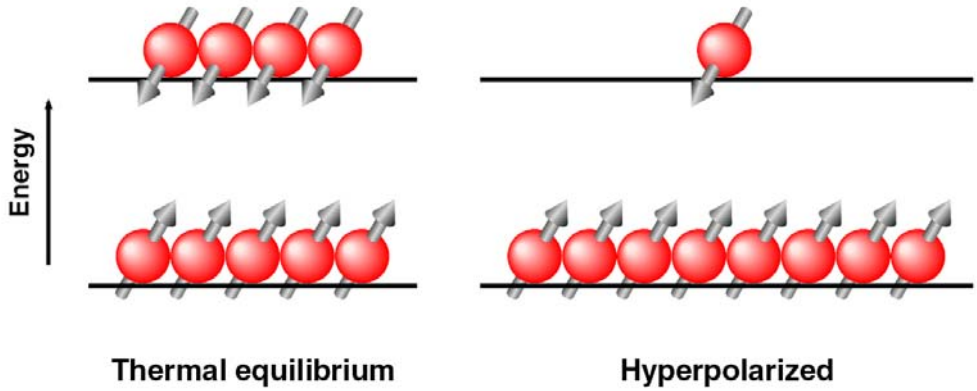

Fig. 2: *Pictorial description of the orientation of the nuclei at thermal equilibrium and in the hyperpolarized state. In the figure, the magnetic field (B_0) is directed vertically upwards.[43]*

The nuclear polarization P (for nuclei with the spin quantum number $I = \frac{1}{2}$) is defined by

$$\mathrm{P} \equiv \frac{\mathrm{N}_{\uparrow} - \mathrm{N}_{\downarrow}}{\mathrm{N}_{\uparrow} + \mathrm{N}_{\downarrow}} . \tag{4}$$

The magnetization $\boldsymbol{M}$, and thus the NMR signal, S, will be proportional to the polarization and the total number of nuclei within the sample $\left(N_0 = N_{\uparrow} + N_{\downarrow}\right)$:

$$S \propto N_0 P . \tag{5}$$

The populations of the energy levels are, under thermal equilibrium conditions, governed by the Boltzmann distribution

$$N_m = \frac{e^{\frac{E_m}{k_B T}}}{\sum_{i=-I}^{+I} e^{\frac{E_i}{k_B T}}} \tag{6}$$

where N_m is the number of nuclei in the state m, E_m is given by (1), and T is the temperature. By combining (4) and (6), it follows that P can be expressed as

$$P = \tanh\left(\frac{\gamma\hbar B_0}{2kT}\right). \tag{7}$$

4.3. Hyperpolarization by brute force and optical pumping methods

From (7), it follows that the thermal polarization increases with increasing magnetic field strength and decreasing temperature. A straightforward, "brute-force" approach to increase the polarization in a sample consists of subjecting it to a very strong magnetic field at a temperature close to absolute zero. The polarizations of selected nuclei at 1.5 T and 310 K, and at 20 T and 4 K (the temperature of liquid helium), are shown in Tab 2.

Tab. 2: *The polarization of selected nuclei at 1.5 T and body temperature, and at 20 T and 4 K.*

Nucleus	Polarization P_1 at 1.5 T, 310 K	Polarization P_2 at 20 T, 4 K
^{1}H	$4.9 \cdot 10^{-6}$	$5.1 \cdot 10^{-3}$
^{3}He	$3.8 \cdot 10^{-6}$	$3.9 \cdot 10^{-3}$
^{129}Xe	$1.4 \cdot 10^{-6}$	$1.4 \cdot 10^{-3}$

The polarization, which is in the ppm range at 1.5 T and body temperature, can be hence increased by a factor of 1000 by cooling down the sample to liquid helium temperature at a field strength of 20 T. If the sample could be brought from 20 T, 4 K to 1.5 T, 310 K instantaneously and without a loss of polarization, it could thus be regarded as "hyperpolarized". Fig. 2 illustrates the difference between thermal equilibrium and the hyperpolarized state.

Eventually, the polarization level of the hyperpolarized imaging agent returns to its thermal equilibrium value at a rate governed by the longitudinal relaxation rate T_1:

$$P(t) = e^{-\frac{t}{T_1}} \cdot \left(P(0) - P_{thermal}\right) + P_{thermal}, \tag{8}$$

where $P(0)$ and P_{thermal} denote the initial and equilibrium polarization values, respectively. The relaxation rate T_1 depends on the chemical and physical environment of the hyperpolarized nucleus, and can range from less than one second to minutes, or even days, for some nuclei. The relaxation rate may differ significantly between in vitro and in vivo conditions. In general, ^{1}H has relaxation rates below 5 s in vivo, whereas the relaxation rates of the other nuclei in Tab. 2 can be more than one minute.

Whenever the hyperpolarization is created outside the body, the available signal will depend on the concentration of the imaging agent after administration. Because only a limited amount of the hyperpolarized imaging agent can be administered, its anticipated concentration is 3 to 6 orders of magnitude lower than the natural ^{1}H concentration in the body. The polarization increase of about 1000 in Tab. 2 will thus not be sufficient to compensate for the low concentration. To obtain polarization levels where the hyperpolarized signal equals, or even outperforms, the ^{1}H signal, the "bruteforce" method would require temperatures in the mK range. Large-scale production of hyperpolarized noble gases (^{3}He and ^{129}Xe) has been proposed using this approach [47]; but due to the great technical challenges and costs associated with the extremely low temperatures, this method has not yet been used for in vivo applications.

However, other techniques exist which sufficiently increase the polarization level of certain nuclei, including ^{3}He, ^{13}C, and ^{129}Xe.

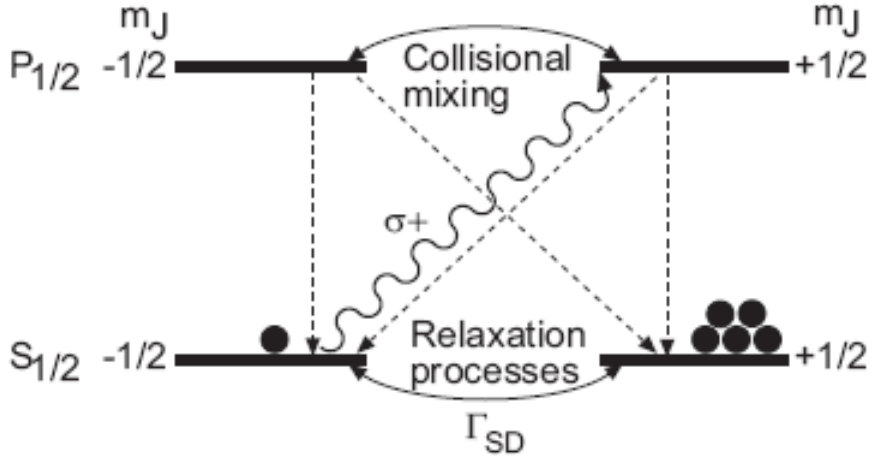

Fig. 3: *Simplified schematic of optical pumping for polarizing the valence electron of an alkali atom. In this schematic the spin of the Rb nucleus is neglected.[44]*

In [48] is showed that angular momentum could be transferred from the electron spins of optically pumped Rb atoms [49] to the nuclear spins of ^{3}He by spin-exchange collisions [48]. The method could be extended to efficiently polarize ^{129}Xe as well [50]. Rb atoms are pumped via the electronic transitions $S_{1/2} - P_{1/2}$ (794.98 nm) and $S_{1/2} - P_{3/2}$ (780.24 nm). For our experiments the D_1 transition line was used ($S_{1/2} - P_{1/2}$). For ^{85}Rb is D_1 transition hyperfine structure in Fig. 5 and for ^{87}Rb is in Fig. 6. [51].

In a magnetic field, the former transition can be driven by circularly polarized laser light (794 nm) to selectively pump the ground-state Rb electrons entirely to the $\left(+\frac{1}{2} or -\frac{1}{2}\right)$ state (Fig. 3). The electronic polarization of the optically pumped Rb atoms is transferred to the nuclei of the noble gas atoms via formation of loosely bound van der Waals molecules or via binary collisions (Fig 4).

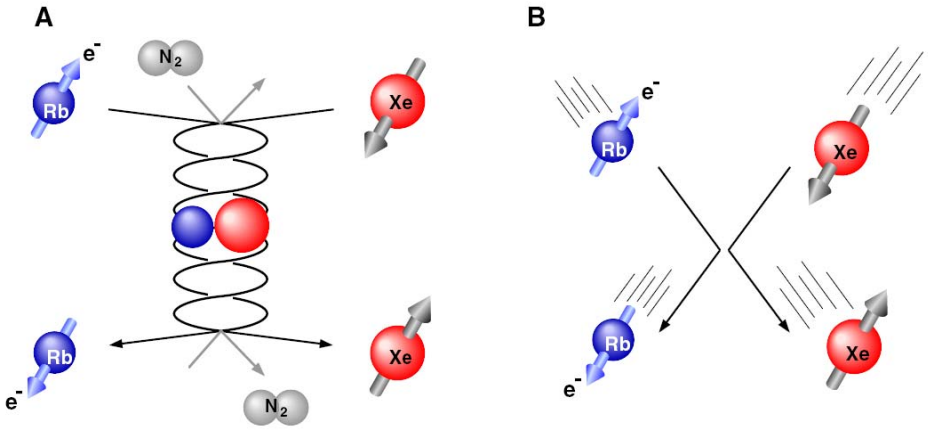

Fig. 4: *Spin exchange between the electronic spin of a Rb-atom and the nuclear spin of a Xe-atom via a van der Waals molecule (A) or via a binary collision (B).[43]*

The former mechanism takes place at low pressure (below ~13 mbar), whereas the latter mechanism dominates above ~500 mbar, or at strong magnetic fields [52].

Viewed macroscopically, the process creates a non-equilibrium polarization of the noble gas nuclei. A classic review of optical pumping methods has been given by [53].

Hyperpolarization of ^{3}He can also be achieved by the method of metastability exchange, first reported in 1958 [54].

In a low-pressure ^{3}He gas (about 1–2 mbar), $^3S_1$ metastable atoms are formed by a weak electrical discharge. By using circularly polarized light, transitions $^3S_1 \rightarrow {}^3P_0$ (1083.0 nm) are induced. Due to strong hyperfine coupling, the nuclei of metastable atoms become polarized. When a polarized metastable atom collides with an unpolarized ground-state atom, a high probability for exchange of metastability exists: the metastable and the ground-state atom exchange their electron shells, while the nuclear polarization remains unaffected. Thus, the collision yields a polarized ground-state atom and an nonpolarized metastable atom. The latter can once more undergo the optical pumping process [55], [56], [57].

Although the theory of hyperpolarizing noble gases by optical pumping was known in the early 1960s, large-scale production has only recently been possible, owing to the development of high-power lasers [58], [59].

The spin-exchange method has the advantage of being able to polarize the gas at high pressures (~10 bar), allowing direct dispensing of the gas from the polarizer,whereas the metastable method only works at low pressure, subsequently requiring cumbersome compression of the gas. On the other hand, the metastable method is faster and can polarize a ^{3}He quantity of 2.5 l (at 1 bar) to ~50% within one hour, whereas the spin-exchange method needs polarization times of around 10 hours for polarizing a quantity of 1 l to ~40%. The spin exchange from Rb to ^{129}Xe (at high temperatures) is more efficient than to ^{3}He. Hence, the spin-exchange technique allows faster polarization of ^{129}Xe: typically, quantities of ~0.5 l (at 1 bar) polarized to ~15% in 30 min were obtained in our laboratory. An overview of the methods for hyperpolarization of noble gases was recently published [60].

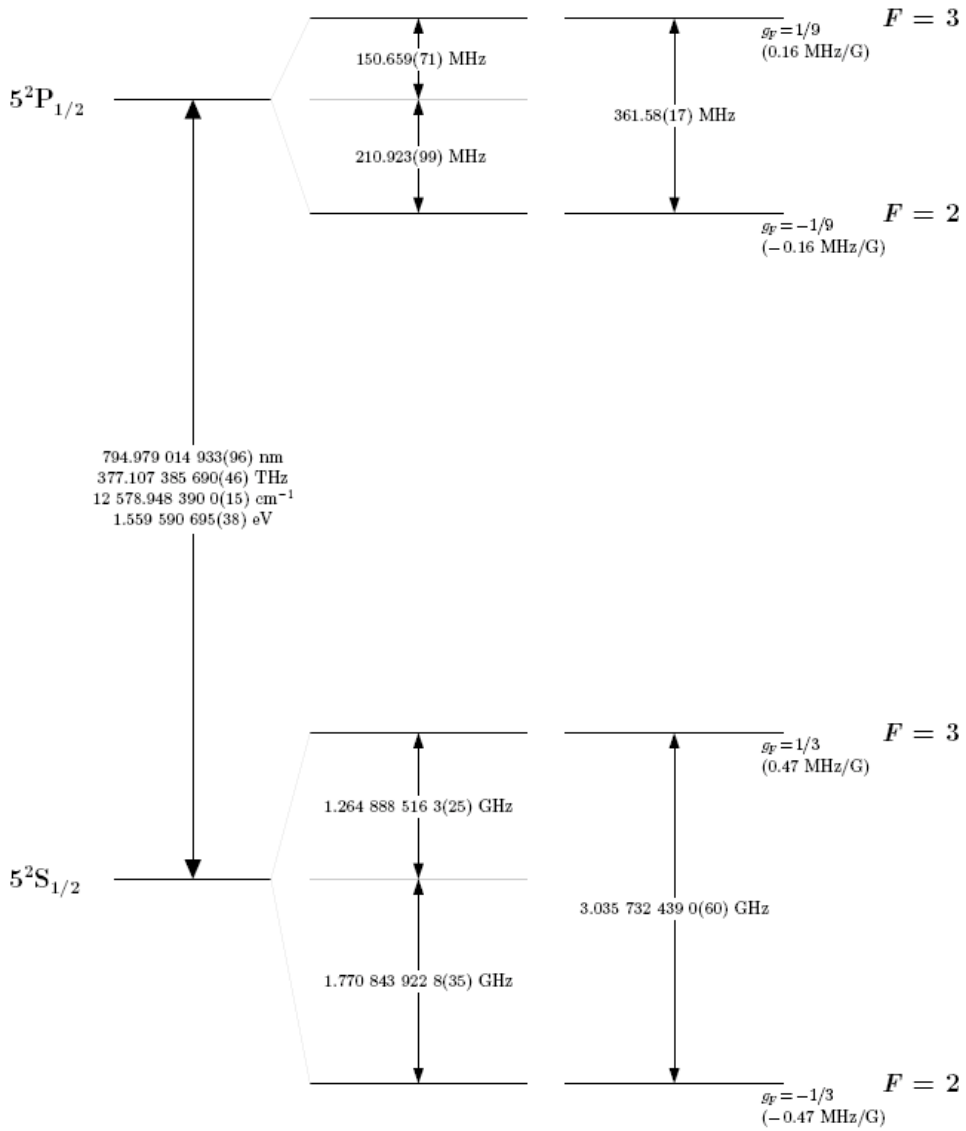

Fig. 5: *^{85}Rb D_1 transition hyperfine structure, with frequency splittings between the hyperfine energy levels.[51]*

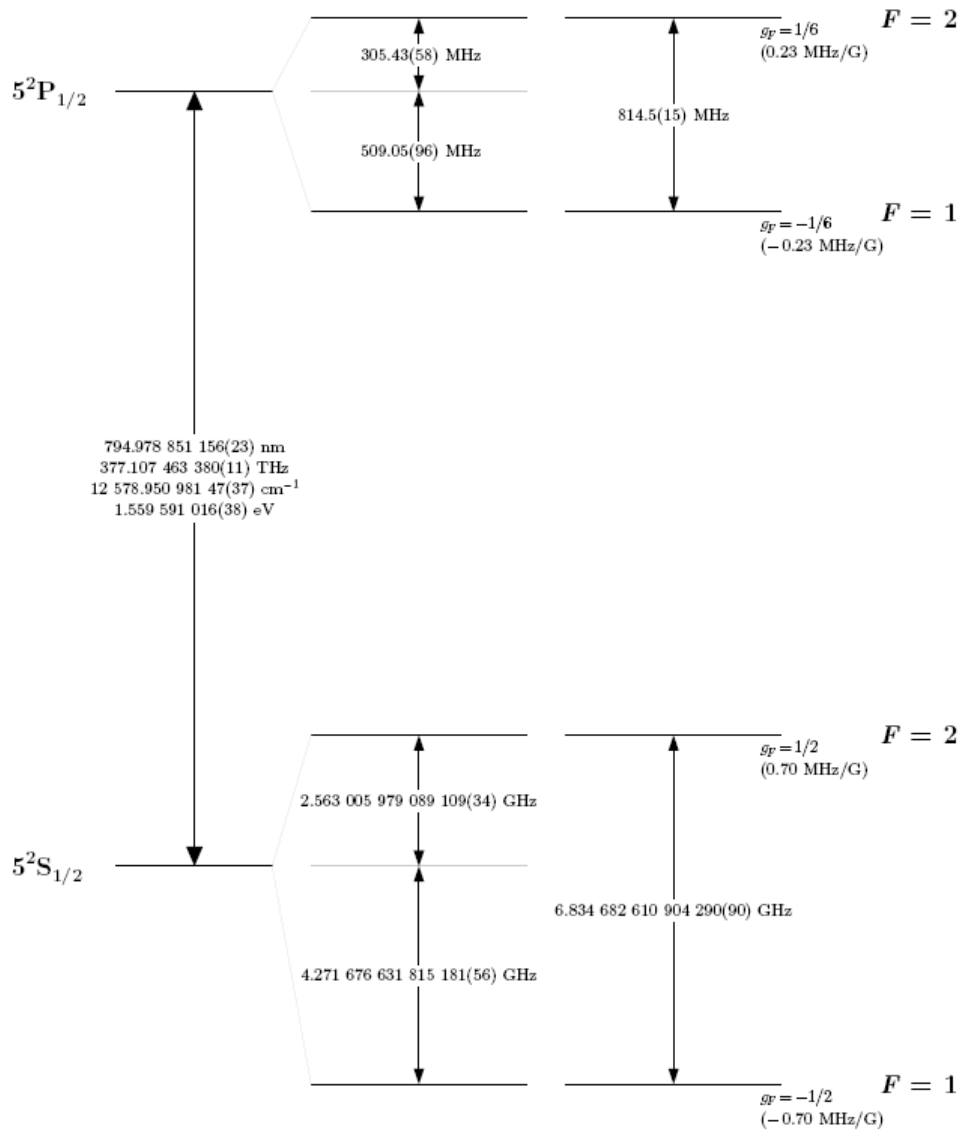

Fig. 6: *^{87}Rb D_1 transition hyperfine structure, with frequency splittings between the hyperfine energy levels. [51]*

4.4. Used NMR techniques

4.4.1. One pulse sequence

For NMR experiments with thermally or hyperpolarized ^{129}Xe was used one simple 90° pulse sequence, which is shown in Fig. 7.

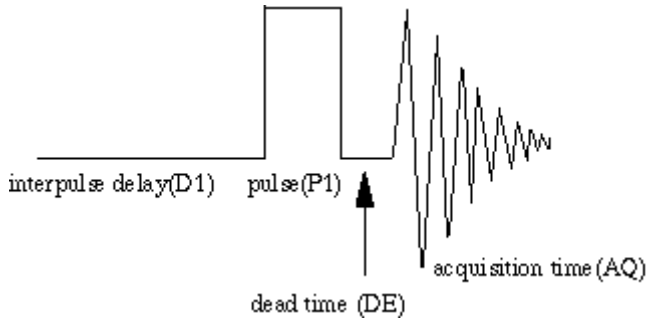

Fig. 7: *Simple one pulse sequence, with 90° pulse.*

In the beginning of the sequence is a delay time. Then RF 90° pulse was applied and then the acquisition time was under way.

The length of 90° pulse was adjusted experimentally to obtain the highest spectral line magnitude. An experimental simple saddle coil was used. The saddle coil was exposed to mechanical manipulation caused by sample insertion and removal, and the coil was retuned from time to time. Because of the mechanical manipulation, the 90° was set before the measurement.

4.4.2. Spectroscopic saturation recovery sequence

The primary use of saturation recovery sequence is to measure T_1 relaxation times, which is quicker than using an inversion recovery pulse sequence. Saturation recovery sequences consist of multiple 90° RF pulses at relatively short repetition times (T_R). An example of a saturation recovery sequence is shown in Fig. 8. After each acquisition (echo) time, presaturation 90° pulses were applied to destroy longitudinal mangetization. The next RF pulse was applied after T_R.

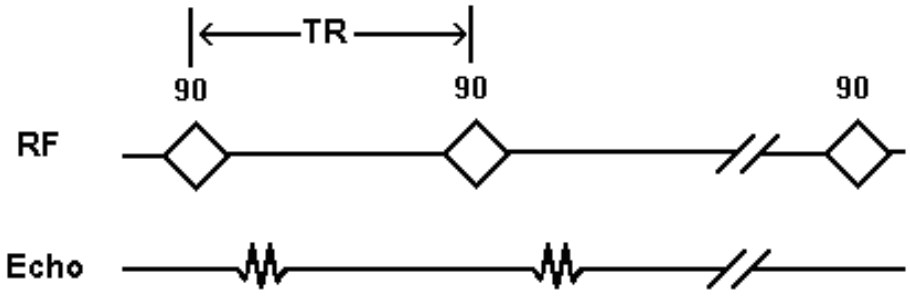

Fig. 8: *Spectroscopic saturation recovery sequence. TR is repetition time, 90 means 90 degree RF pulse, Echo is for data acquisition. Modified from [61].*

5. Functional parts of experimental setup for xenon hyperpolarization

The experimental setup for xenon hyperpolarization in sealed glass cell was based on laser diode, which is described in subchapter 5.2. The NMR part was used for studying the ^{129}Xe hyperpolarization rate, and is described in subchapter 5.3. The part, which was used for sample creation is described in subchapter 5.1 as a vacuum part. The same vacuum part was further used in an experimental setup for xenon hyperpolarization under continuous flow, even though it was little bit modified, see chapter 6.3. The block diagram of the experimental system is shown in Fig. 9.

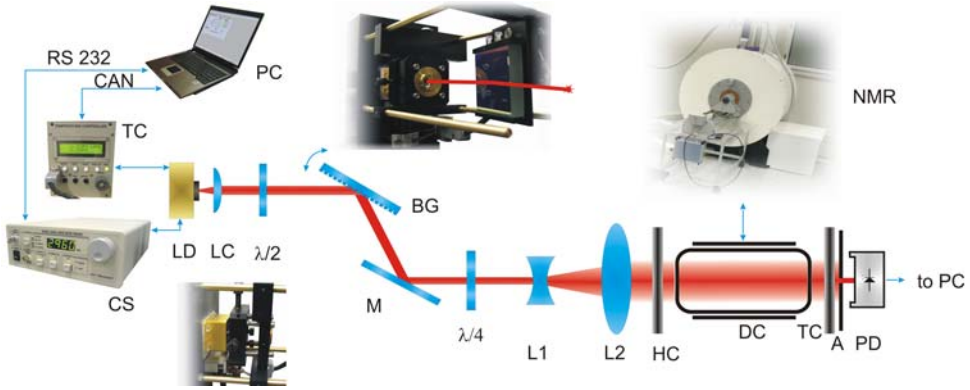

Fig. 9: *Experimental set-up for xenon hyperpolarization. TC is temperature controller, CS is current source and PC is personal computer. LD is high-power laser diode; LC is aspheric collimating lens; l/2 is retardation half-wave plate; BG is diffraction grating in Littrow configuration. M is mirror; λ/4 is retardation quarter-wave plate and L1 and L2 are lenses formed optical telescope. HC are Helmholtz coils; DC is detection coil; TC is target cell; A is aperture; PD is photodetector and NMR is 4.7 T nuclear magnetic resonance system.*

5.1. Vacuum part

The vacuum part could be divided into several parts, which are described in following sections. The main component was turbomolecular drag pumping station, which was used for the vacuum preparation. With this pumping station the part containing special gases for samples preparation was also connected. For simple connections and for simple joints Teflon or Stainless Steel tubing and Stainless Steel or Viton sealed plastic stopcocks and valves were used. For all the glass parts Simax glass was used. Other used materials will be specified whenever needed.

5.1.1. Turbomolecular drag pumping station

In all of the experiments, the vacuum part was based on turbomolecular drag pumping station TSH 071 E (Fig. 10) consisting of diaphragm pump MVP 015-2 with limiting pressure ≤4.5-3.5 mbar (450-350 Pa) and turbomolecular drag pump TMH 071 P limiting pressure $<1\cdot10^{-7}$ mbar ($<1\cdot10^{-5}$Pa). Single gauge control unit TPG 261 and vacuum gauge PKR 251 in ranges from 1000 mbar ($1\cdot10^{5}$ Pa) to $5\cdot10^{-9}$ mbar ($5\cdot10^{-7}$ Pa) were used for vacuum measurement. All vacuum equipment used in the experimental setup was manufactured by Pfeiffer Vacuum GmbH. Some vacuum fittings and valves were home-made or by Lavat a.s., Chotutice.

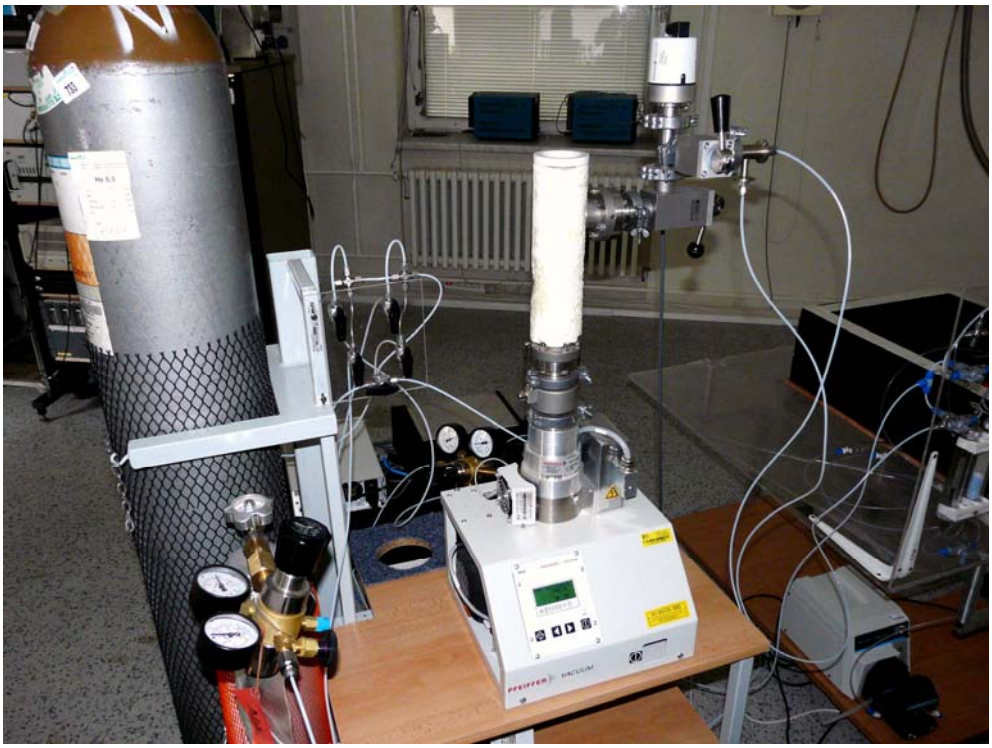

Fig. 10: *Turbomolecular drag pumping station TSH 071 E.*

5.1.2. Target cell and vacuum apparatus design

To conduct experiments with Rb optical pumping and Xe hyperpolarization, a special target cell had to be made. It is shown in Fig. 11.

The cell is made from borosilicate glass which was chosen because of its price. The cell is considered to be consumable and hence it has to be a low-cost product. The price of the borosilicate cell is lower by approximately two orders in comparison with the quartz glass cell. The flat windows of cell are made from borofloat and both of them are fused to the simple cylinder. The optical quality of the borofloat windows is not as high as the optical quality of fused silica windows but it is sufficient for this application. The borofloat windows were used because of their high flatness and low price. Active length of the cell is 92 mm and the inner diameter is 35 mm. The target cell was completed at the ISI AS CR, v. v. i. under supervision of Dr. Petrů and his group who has a great experience with a production of varied cell types, mainly the iodine cells for iodine-stabilized He-Ne lasers [68] which are made from quartz glass.

Fig. 11: *Target cell. The silver metal pieces – its rubidium in solid state (at the room temperature).*

After the cell was completed, it was cleaned with acetylene. The ampoule with small amount of Rb was attached to the cell with a break-seal. The amount of Rb had to be sufficient to reach of the saturated Rb vapour in the calefactive target cell (in this case it was approximately 5 mg). The cell was connected to a vacuum apparatus by a glass tube. The vacuum apparatus is sketched in Fig. 12. The apparatus has to be evacuated because Rb oxidizes in the atmosphere and becomes explosive. After the cell was connected, the turbomolecular drag pumping station, which is described in chapter 5.1.1., was turned on. During the evacuation process, the cell together with the apparatus was heated to the temperature of about 120°C to be degassed. At least five hours of pumping at this temperature followed by a few hours of pumping of the cool-down apparatus are necessary to reach high vacuum inside the cell. This process evacuated the apparatus down to a pressure of 8.10^{-5} Pa. The evacuated space is subsequently overpressurized by the mixture of xenon (26% of ^{129}Xe), helium ^{4}He and nitrogen N_2. Then, the glass vacuum valve between the cell and the apparatus is closed, the cell is heated to approximately 100°C and then break-seal of the Rb ampoule is broken. At the temperature higher than 38.85°C [69], Rb becomes a liquid and the Rb vapour is released. The vapour together with Xe and the other buffer gases makes the desired mixture of gases for xenon hyperpolarization.

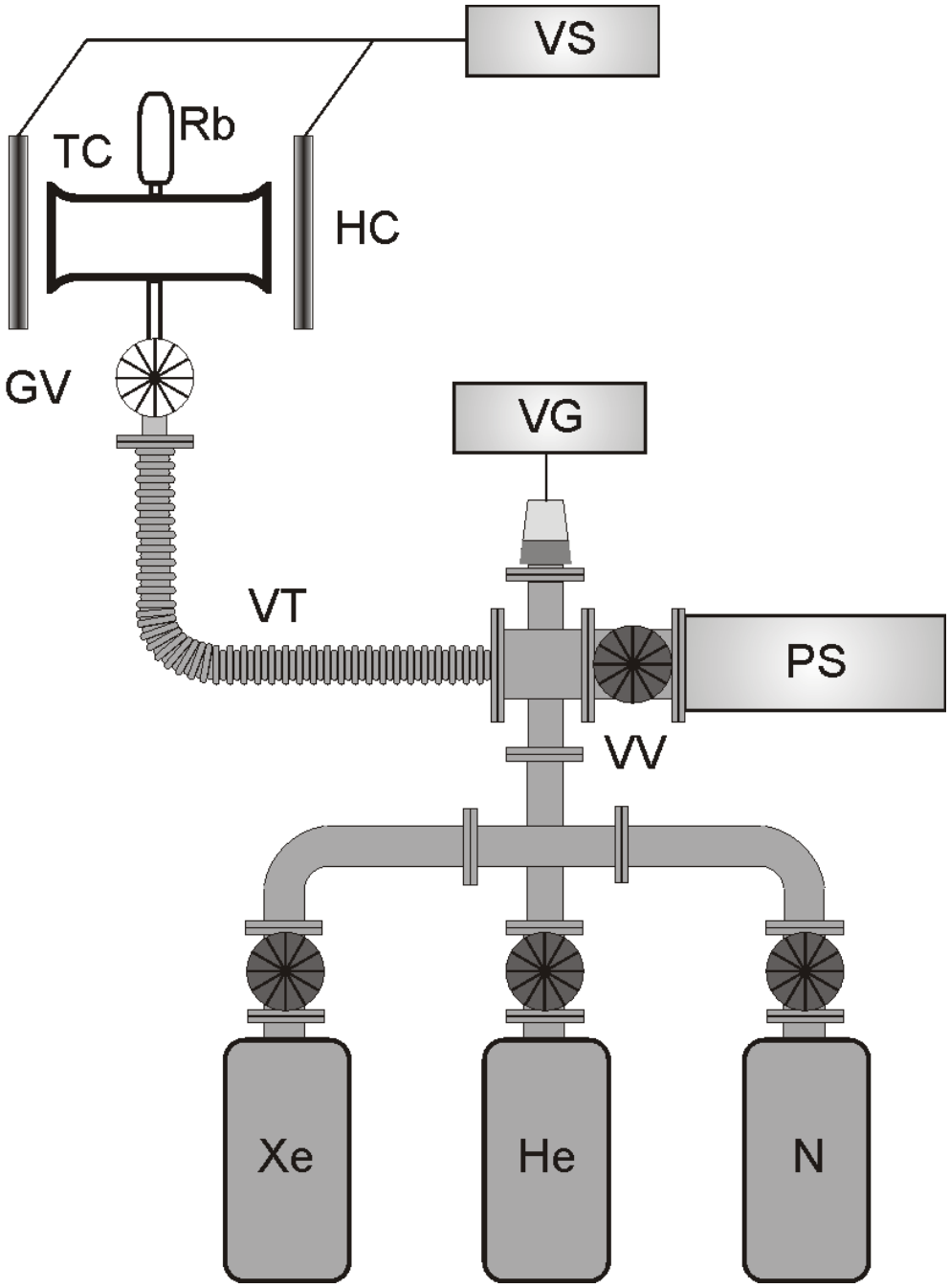

Fig. 12: *Vacuum apparatus used for the target cell evacuation. TC is target cell, Rb is glass ampoule with rubidium, GV is glass vacuum valve, VT is vacuum tube, VV is vacuum valve, VG is vacuum gauge, PS is turbomolecular drag pumping station, Xe is xenon bottle, He is helium bottle and N is nitrogen bottle. HC are Helmholtz coils and VS is DC power supply.*

Several modification with experimental arrangement sketched in Fig. 12 using the procedure described above were done. Different kinds of valves and couplings between the cell and the apparatus were tried to be applied. The only requirement was, that the valve has to be made from non-magnetic and a non-metal material, because a magnetic material would disturb the homogeneity of the magnetic field the cell is placed in, and a metal material would depolarize the hyperpolarized xenon. First of all, a Teflon valve was applied in combination with a plastic tube to connect the cell and the apparatus together. This material was preferred because the plastic tube guaranteed the flexible

connection of the glass cell and stainless steel apparatus. The flexible connection decreased the probability of the cell damage, but the plastic material was not suitable to be applied in a high-vacuum system. Once the Rb oxidized due to insufficient air-tightness after the Teflon valve was heated. The Rb oxidization is an irreversible process. In this case, the oxidized Rb was liquid even at the room temperature and it changed its color from silver to metal-yellow (like gold). In the next developmental step, the glass vacuum valve and glass tube were used to connect the target cell and the apparatus. This setup was developed and tested. It was found out, that the ground part between the stopcock and the yoke, even though it was vacuum lubricated, was leaking.

Consequently, we decided to make a completely sealed target cell for the first experiments with xenon hyperpolarization. The manufacturing procedure was the same as the one described above, except for the part with the vacuum valve enclosing. After the evacuation and over-pressuring by the mixture of Xe and the other buffer gases, the glass tube between the cell and the apparatus was cut off, and the cell was sealed up. If the pressure of the buffer gases is higher than atmospheric pressure, the cell has to be cooled down by liquid nitrogen to reduce the buffer gas pressure under atmospheric pressure before one can seal up the cell. Then, the break-seal was broken and the cell was heated to approximately 100°C so that the Rb vapour was released. The practical experiments with xenon hyperpolarization are described in Chapter 6.

The target cell is placed into a Helmholtz coil system designed to generate a homogenous 10 mT magnetic field with homogeneity of $2.18 \cdot 10^{-4}$. The mentioned system parameters are sufficient for the Rb energy levels splitting (Zeeman effect). The system is supplied by highly precise stabilized DC power supply Agilent 6654A (Fig.22 - at the bottom, in the middle)

5.1.3. Glass operating segment for xenon hyperpolarization under continuous flow

Experimental setup for xenon hyperpolarization under continuous flow has entirely different demands for a configuration in comparison to the method with sealed cell, but the principle is the same. In continuous flow regime, the entities entering into the system are noble gas (^{129}Xe) to be polarized, quenching gas (N_2), and possibly helium (He) as a buffer gas, and rubidium to be optically pumped. The leaving entity is: hyperpolarized noble gas in a gaseous or a frozen state, to be used or preserved for later use. Nitrogen and buffer gas return into the continuous flow process, because the temperature to freeze xenon is lower than their freezing point. Rubidium vapours were cooled down in a water bath in temperature above 0-5°C.

Other parts participating in the continuous flow were: tubes as a gas distribution system, peristaltic pump, hyperpolarized xenon storage tank, flow meter and NMR probe, which will be described in one of the following chapters.

The important and interesting construction of a part for optical pumping, which consists of three glass parts is shown in Fig. 13.

The first part was based on a chemical glass radiator with coils. A small rubidium ampoule with a break-seal was attached to this part, using the same technology that is described in chapter 5.1.2. The liquid rubidium was transferred into the radiator coils. The radiator was heated by the hot-air pistol to 100°C through silicon tube reduction (see Fig. 13 – a piece of white silicon reduction tube is visible in the bottom right corner).

The second glass part looks like a target cell described in chapter 5.1.2. with the same active dimensions. It was heated by the residual heat flow getting out from the radiator.

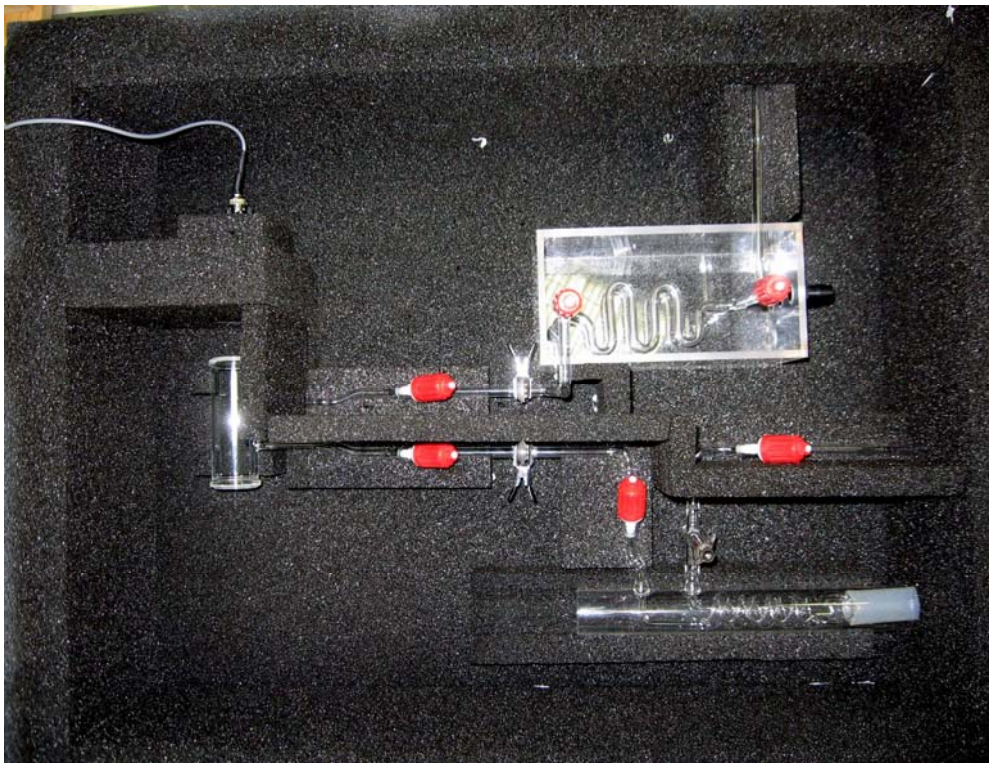

Fig. 13: *The Foamglas box with optical pumping glass parts. At the bottom of the picture, there is the chemical radiator with coils. In the middle is the target cell (above the cell is visible photodetector cable). On the top of the picture a small acrylic bath is visible – as well as a rubidium condenser with five Simax arcs. The red parts are Rotaflo stopcocks. In the picture two metal clips, which connect spherical grinded joins together, are also visible.*

The third glass part was made from a glass tube, modified into the serpent with five arcs. This section served as a rubidium condenser and was immersed in a cold water bath. The water bath was connected by plastic tubes with a standard bucket, in which the water was cooled down by two spirals. The water reservoir was situated under the table, as shown in Fig. 10. The bucket with a nominal volume of 10 l is used as a water reservoir. The reservoir was covered with an acrylic lid, on that was mounted a small pump EHEIM 1048, the main component of the primary circuit of the rubidium condenser. The secondary circuit was based on Ultra-Kryostat MK 70 and was connected with the water reservoir by red plastic hoses. The temperature was controlled by two old serially connected hollow copper heating spirals taken from an old thermostat (Fig. 14).

On each of the three described glass parts were attached two Rotaflo stopcocks with Teflon valves, which allowed both sides of each of the three parts to be sufficiently closed, when disassembly was needed. The parts were connected together by glass pipes with internal diameter 5 mm and ended by ground-semispherical joints and connected by Stainless Steel clips.

The above described glass construction was placed in Foamglas® box - a black box in Fig. 13. - which is a great ecological cellular glass thermal insulation material.

Fig. 14: *Water reservoir (left hand side) – the bucket with acrylic lid, in which is a thermometer. Small pump Eheim 1048 is mounted on the lid. Two spirals are connected by red hoses with Ultra-Kryostat MK 70 (right hand side), which works as a cooler.*

5.2. Optical part

The important part of the system for HpXe production is the setup for optical pumping of rubidium atoms. In the majority of laboratories dealing with the HpXe production, semiconductor laser system for optical pumping of Rb is used. Usually, it is a system with enormous optical power output (up to a few hundred watts) and broad emission spectrum (a full width at half maximum is a few nanometres). These systems are commercially available and allow the continuous HpXe production but only a fraction of the total optical power is employed in the Rb optical pumping process. It is because of the broad laser emission spectrum which is much wider than the Rb vapour absorption line. The extremely excessive optical power is not only wasted, but also causes potential risk to the maintaining staff and has to be thus somehow safety pumped.

In experiments described in this thesis, a high-power narrow-band semiconductor laser system which allows optical pumping of Rb with much higher efficiency than the mentioned commercially available systems was used. Such an arrangement should be compact and portable enough to move it close to the site where NMR or MRI experiments with HpXe will be performed.

For the pilot experiment with optical pumping of Rb atoms, the commercially available Ti:Sa laser (Coherent, model 899-01) was used [53]. The laser is tunable in a wide wavelength range. Its optical power output depends upon the power of the pumping beam and also on the quality of the whole laser system adjustement. In our case, the maximum value is approximately 1 W. One of the most important parameters of the laser used in a spectroscopic application such as optical pumping of Rb, is the emission linewidth. The Model 899-01 has two primary operating regimes, but continuous laser frequency tuning is possible only in the broadband regime. In this case, the Ti:Sa laser emission linewidth is 25 GHz which is broadly in accordance with the rubidium absorption linewidth.

Due to its spectral properties, the mentioned Ti:Sa laser is suitable for Rb optical pumping. On the other hand, the laser is a system with opened optical resonator and it makes it sensitive to fluctuations of the refractive index of air inside the optical resonator which induce the variation of the laser frequency, and also to dust particles, which presence in laser resonator leads to losses in the laser resonator and falling of the output optical power and also induces fluctuations of the output optical power. Because of this reasons, the Ti:Sa laser is not usable outside of the dust-free and air-conditioned laboratory.

For experimental and practical use, semiconductor lasers seem to be the best choice [54, 55]. Semiconductor lasers are nowadays widely spread in all laser applications. They are relatively cheap, simple in operation, and also possible with high output optical power. For this reasons, a high-power type of semiconductor laser was used.

A major part of the research described in this work was conducted using a high-power laser system, instead of the Ti:Sa laser. The laser system is based on a semiconductor laser, specifically on a single stripe high-power laser diode. The principal disadvantage of this kind of semiconductor laser is that its high output optical power is spread in wide spectral range; typically it is about 1000 GHz.

To compare different kinds of lasers, a quantity known as “power spectral density” is used. It represents the optical power concentrated in a specific spectral range – in our case it could be the Rb absorption linewidth. From this point of view, the high-power laser diode with a few watts of output optical power is far less advanced in comparison with the Ti:Sa laser. Fortunately, there are a few useful ways to increase the power spectral density at desired spectral ranges.

The simplest way to make the solid-state laser emission line (laser bandwidth) narrower is to chill the active medium in order to reduce thermal broadening. Unfortunately, it is not very effective way of reducing the bandwidth and on top of that it changes the central wavelength of the emitted radiation.

An alternative approach is to replace one of the laser resonator mirrors with a grating [56, 57, and 58]. A grating is an interferometric device that diffracts different wavelengths at different angles. When it is aligned correctly at the end of the resonator, it will reflect back to the active medium only the light at the center of the laser transition line. Thus, lasing bandwidth is again reduced to the bandwidth of the resonator’s round-trip gain. Either optical prism or diffraction grating could be placed outside the laser resonator. In this case, a part of the laser radiation is lost. Nearly as much laser power can be produced in a narrow bandwidth as in a wide bandwidth, when the bandwidth-limiting device is inside the laser resonator. As for laser diodes, typically one of the resonator mirrors is coated with antireflective material and replaced by an external diffraction grating is used. This setup is called extended cavity laser (ECL).

5.2.1. Laser for optical pumping of Rb atoms

The block diagram of the laser system used in Rb optical pumping experiments is shown in Fig. 15 [59]. The main part of the arrangement is the high power laser diode S-λ-3000C-200-H (Coherent). The maximum output CW power is approximately 3 W, the central wavelength is about 797 nm at the temperature 25°C and the LD emission linewidth is about 1 THz.

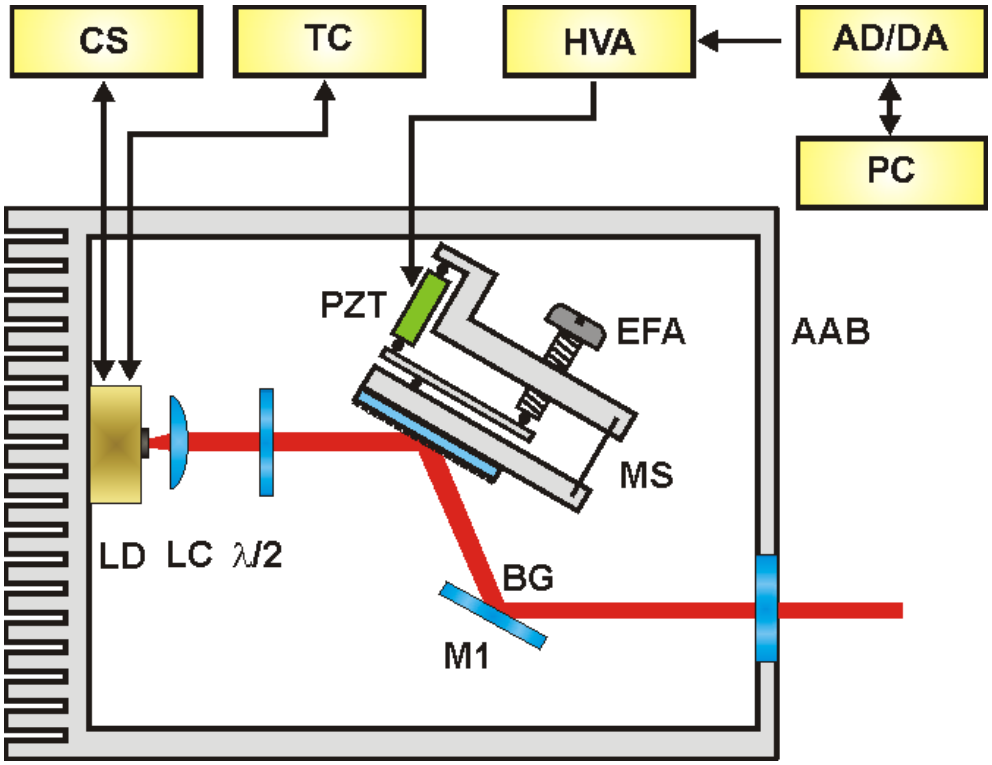

Fig. 15: *Fig. A: Block diagram of the designed laser system. CS is current source, TC is temperature controller, HVA is high voltage amplifier, AD/DA is AD-DA converter and PC is personal computer, LC is aspheric collimating lens, λ/2 is retardation half-wave plate, BG is diffraction grating in Littrow configuration. PZT is piezoelectric transducer, EFA is extremely fine adjustment screw, MS is flexible plate. M1 is mirror and AAB is aluminum alloy box.*

The output beam is collimated with aspheric, high NA lens. To achieve the laser diode emission linewidth reduction, a diffraction grating was used in simple Littrow configuration as a wavelength selective feedback which was optimized by a retardation half-wave plate exploiting the polarization sensitivity of the grating. In the experimental setup, the holographic diffraction grating 2400-line/mm with Littrow angle 72.4° was used.

Due to variability of the final laser system, the bottom plate of the ECL box is used as breadboard which allows positioning of the optical components in ample range. A laser diode is mounted on the rear plate which serves as a passive cooler. All dural plates are black anodized to suppress unwanted reflections. The plates (except the top one) are connected together by special glue for aluminum alloy, which is the plate material. Glue was preferred to screws because the glued box is more similar to the one made from duralumin bulk. The real view of the compact laser system is in Fig. 16.

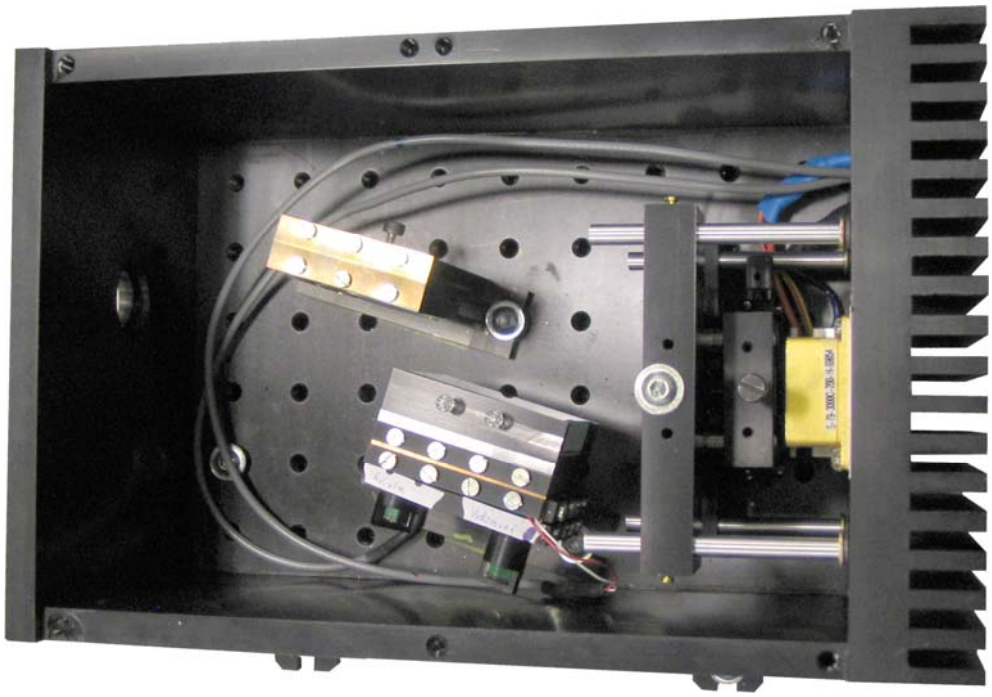

Fig. 16: *Compact laser system with high-power laser diode.*

With the experimental setup shown in Fig. 15, we were able to reduce the laser diode emission linewidth more than 10 times, from 732 GHz to 69 GHz full width at half maximum. The power loss was 49%, from 3.14 W to 1.60 W.

The laser emission spectrum was measured by a commercially available DK 480 ½ meter monochromator equipped with USB 2.0 CCD line camera (Thorlabs). The monochromator resolution is 0.04 nm. The laser spectrum recorded with the camera is processed by software specially designed in Matlab. The obtained laser diode emission spectrum in comparison with the ECL system spectrum is shown in Fig. 17. The recordings of line profiles are scaled by normalizing with respect to the overall optical power which was measured independently. The measured line profile of the ECL laser is shown on the background of the original emission profile of the LD. To put them into scale the reduced line profile is multiplied by the constant R (9) to equalize its optical power spectral density with the one of the original emission profile.

$$R = \frac{P_r \cdot S_o}{P_o \cdot S_r}, \tag{9}$$

where P_r is output optical power of the ECL, S_r is the integrated surface of the line profile, P_o is original LD output optical power and S_o is the original LD integrated surface of the line profile. The gain of the camera is the same in both cases.

The parameter R is simply a power spectral density enhancement ratio at the desired wavelength. It is the parameter of the ECL system and describes the increase of the peak normalized power spectral density achieved by the ECL. It is the ratio between the ECL peak power spectral density and the original LD peak power spectral density.

Generally speaking, the parameter R is mainly reflective of the quality of the ECL system adjustment. Its value widely varies during the system settings process. To reach the best state, which is usually adequate to $R = 3$, the system has to be tuned extremely

finely and precise. I reached of the ECL system settings quality for which is the parameter *R* equal to 3.7.

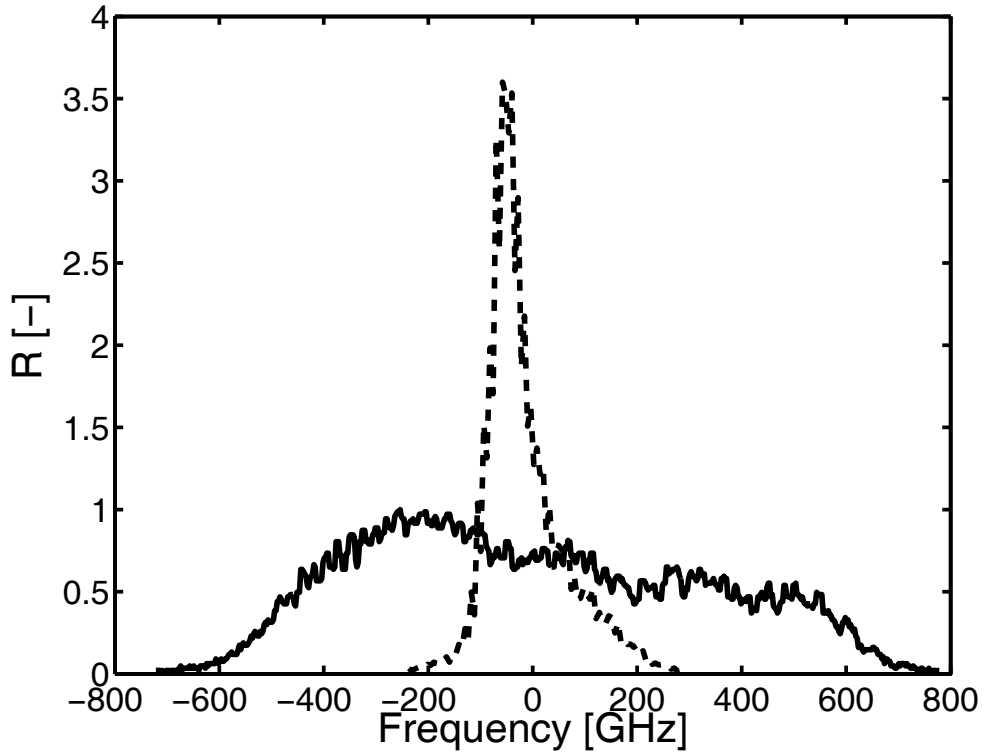

Fig. 17: *The laser diode emission lines. The solid curve is the LD original emission line and the dashed curve is the reduced emission line.*

The first experiment was conducted with the heavy, non portable Ti:Sa laser, which is even more importantly, sensitive to dust. Therefore, the first experimental device was placed near Ti:Sa laser in overpressured box that ensured a clean Ti:Sa optic system without lowering optical laser power in time. In the second step, laser diode at free running and ECL regime was used.

5.3. NMR part

The main part of the NMR system is a small bore horizontal magnet type MRBR 4.7 T / 200 MHz with shielded gradients (Fig. 18) by Magnex Scientific Ltd. (now a part of Varian Inc.), which has been in our institute since 2000. As gradient amplifiers Techron 7700 by AE Techron, Inc. are used.

The original electronics were constructed with Kalmus 137C radio frequency amplifier and PTS 500 frequency synthesizer and other home-made electronics.

The RF electronics, system control, data acquisition, and processing software modules have been modernized since 2007 employing progressive technical solutions based on digital signal synthesis and digital signal processor.

In principle, the electronics are based on MR6000 by MR Solutions Ltd. Some specifications fit directly to our system and requirements. The electronics are configured for 4.7 T magnetic field. The dual channel PTS D310 frequency synthesizer, a set of high frequency filters, two preamplifiers, four receivers and some other

modifications to the original MR6000 are our chosen adjustments for operating a multinuclear system (Fig. 20)

As a radio frequency amplifier 5T1000M by CPCAmps is used.

A RF coils are mostly home made. The ^{129}Xe RF coil is shown in Fig. 19.

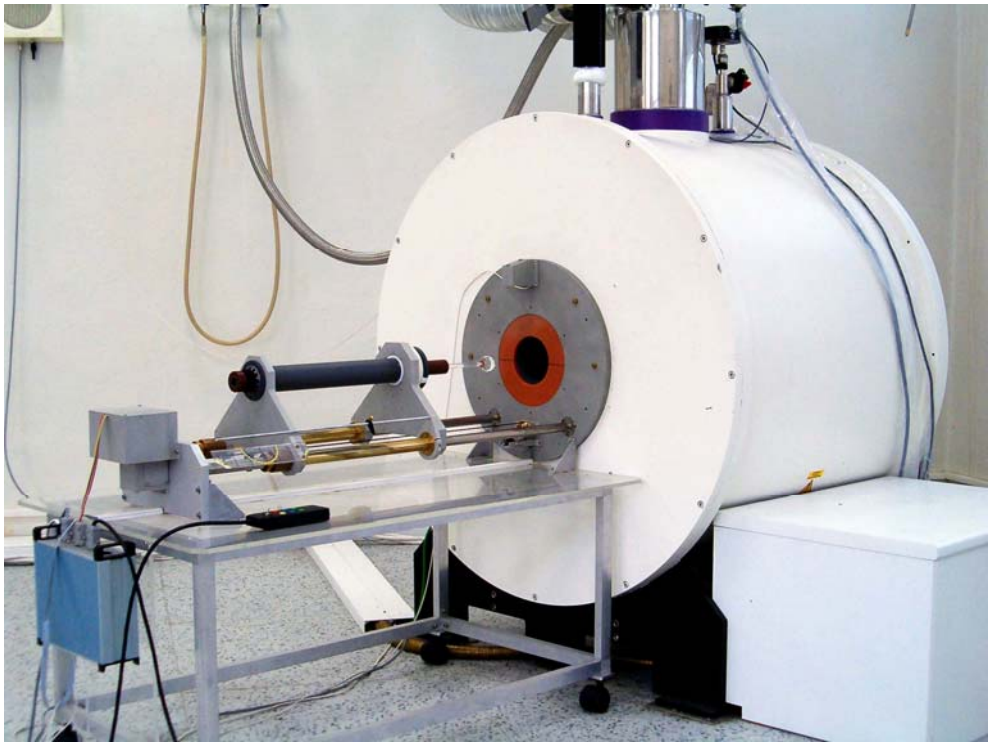

Fig. 18: *4.7 T, 200 MHz NMR system with traversing sample table.*

Fig. 19: *Small ^{129}Xe saddle RF coil with a sample.*

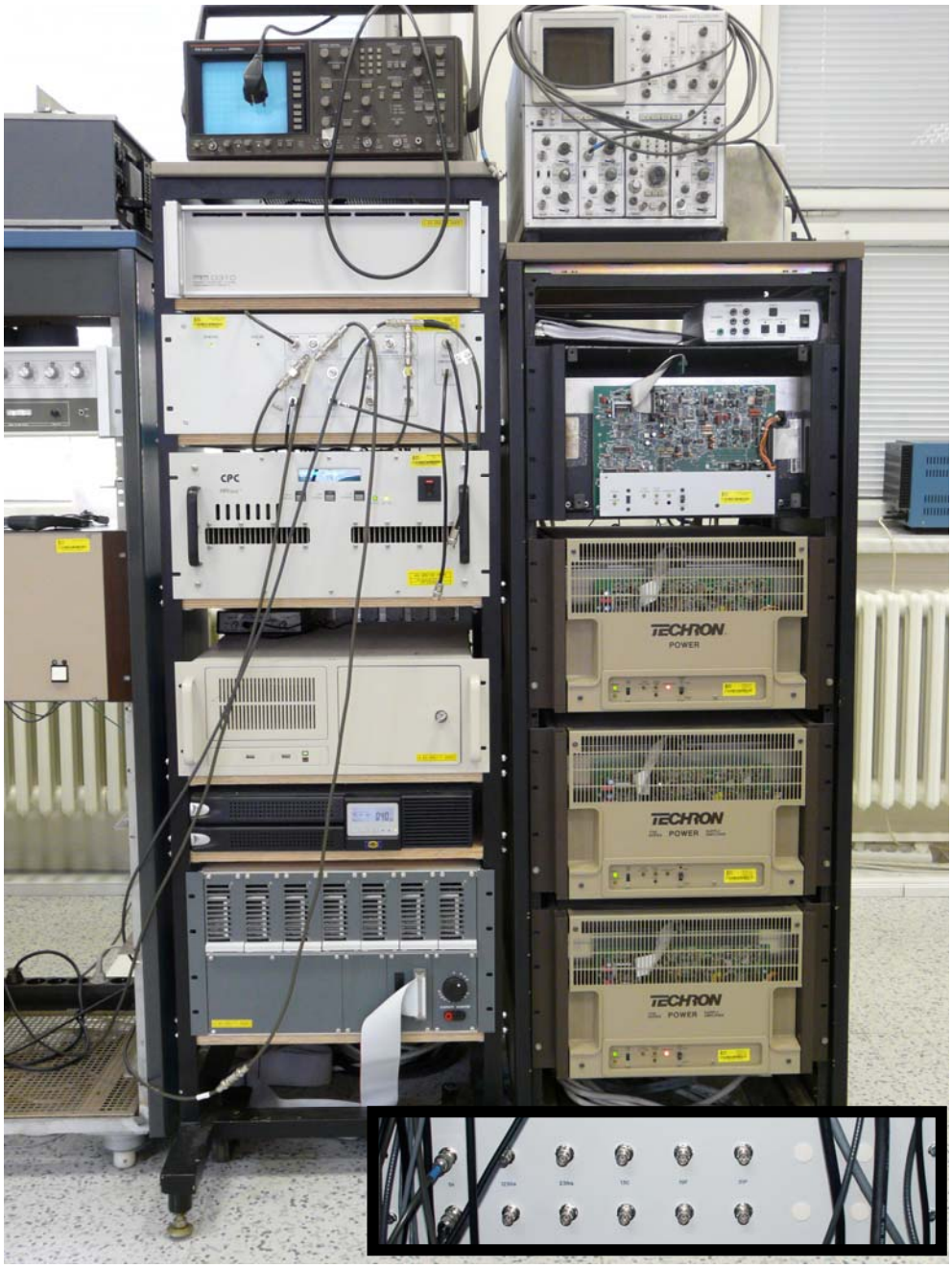

Fig. 20: *In the left rack is from above downwards: PTS 0.1 - 310 MHz frequency synthesizer, MR Solutions Ltd. spectrometer, CPC 1 kW amplifier, control PC, and shim multiple current source. In the right rack are gradients current sources. The nuclei HF filters are shown in the bottom right corner.*

5.3.1. Small portable NMR system

In a quest for a small and portable xenon polarization system, a small NMR experimental system (Fig. 21) was also designed, consisting of a home-made pair of Helmholtz coil, generating the magnetic field up to 10 mT with homogeneity of $2.18 \cdot 10^{-4}$, supplied by highly precise stabilized DC power supply Agilent 6654A [77], and home-made small RF system with RF saddle coil.

The RF system bandwidth is from 9.7 kHz (4096 decimation) to max 156.25 kHz (256 decimation). The minimal step of pulse time is 0.0005 ms and minimal step of time delay is from 0.1 ms to 1600 ms.

The electronic box is connected to notebook or PC through USB interface and controlled by the home-made software programmed in Matlab. The electronics and saddle coil are projected and assembled for ^{1}H resonant frequency 116.8 kHz at 2.74 mT what correspond to ^{129}Xe resonant frequency (117.77) kHz at 10 mT.

Fig. 21: *The small NMR experimental system. Helmholtz coil (left hand side), electronics (above) and current source (bottom) (in the middle), and control unit – PC (right hand side).*

6. Experimental results

6.1. Thermally polarized xenon

First, experiments with the thermally polarized natural xenon (with natural abundance 26.4% of ^{129}Xe) were conducted.

The first set of samples based on glass capsules closed with plugged plastic tube was created. These capsules were filled with natural xenon or xenon-oxygen mixture or with paraffin oil or cyclohexane impregnated by natural xenon. Oxygen, paraffin oil and cyclohexane were used to shorten presumed gases long relaxation time. The samples were simple Simax glass cylinders of 14.6 or 26 mm in diameter and of around 50 mm in length. The samples were filled with natural xenon under different partial pressures and with previously mentioned kinds of mixtures. Capsules were inserted into magnetic field of 4.7 T NMR system to achieve a thermodynamic equilibrium state given by Boltzmann distribution. After several hours glass capsules were inserted one by one into a small saddle coil and one pulse sequence was applied. All samples were without signal. This might have been caused by the fact that the amount of diluted xenon in paraffin oil or in cyclohexane was not sufficient, saddle coil's small sensitivity to this type of experiment or because the xenon gas or gas mixture (in case with oxygen) was plugged without being frozen with liquid nitrogen and not (over)pressurized enough.

For the second attempt, sealed capsules with 2 and 0.5 atm of natural xenon were prepared. These samples were frozen with liquid nitrogen before sealing and gave signal after achieving thermodynamic equilibrium in 4.7 T NMR system. The signal of ^{129}Xe spectral line was proportional to the total pressure and volume of xenon gas.

In a few subchapters some of the experimental results are described and presented.

6.1.1. Natural xenon spectral line magnitude

After the experience described in the previous chapter, the sealed glass samples were prepared. The effort was to prepare samples preferably of around 1 atm of gas mixture, or greater, because of a greater chance to obtain measurable signal. The samples had around 50 mm in length and 26 mm in diameter. The gas pressure under 1 atm was defined by a pressure meter. The samples with gas pressure greater than 1 atm were frozen before sealing. Therefore, the total pressure could have been a little bit greater than the one previously described, because of a small residual inlet volume between the sample and the valve. All samples were evacuated before filling in the orders of 10^{-3}-10^{-4} Pa.

The simple pulse sequence was used, with pulse length 80 μs, strip width (SW) 50 000 Hz, number of samples (SI) 8 k, LB = 10. The FWHM (full width half maximum) of spectral lines size in Tab. 3 was measured without LB.

Tab. 3: *Thermally polarized xenon – signal amplitude results after several hours.*

Sample no.	Pressure [atm]	Magnitude [-]	FWHM [Hz]	Spectrum integral [-]
1	>0.2	15.4	-	122.5
1	>0.2	18.4	7.8	-
2	0.6	0.9?	-	5.4?
3	0.9	2.3	-	21.5
4	0.3	0	-	-
5	2	4.4	-	-
6	>1	68.2	7.7	-
7	>2	141.7	7.2	-

In Tab. 3 there are shown results of the first experiments with small sealed samples and thermally polarized natural xenon.

It appears from spectrum integral ratio between sample no. 3 and 1, that the real pressure in sample no. 1 could have been about 5 atm. This roughly inaccurate information was not remeasured and because of the character of these first experiments, this was not considered a fundamental imperfection.

The pressure in samples no. 2, 3 and 4 is sufficiently defined and the results are reliable.

The pressure in sample no. 5 was 2 atm before being frozen. The inner wall of this sample was covered with Teflon.

The pressure in samples no. 6 and 7 is also specified before the sample was frozen and sealed, so the real pressure could have been a little bit greater. With sample no. 7 the best result had been reached and because of its strong signal, this sample was used as a reference, or for the saddle coil retuning when needed. For sample no. 7 the T_1 relaxation time was measured by saturation recovery method. The maximum spectral line magnitude was 143.4. Measured dates (Tab. 4) were fitted (Fig. 22) and T_1 relaxation time 13.6 min (817.5 s) was enumerated in Matlab.

Tab. 4: *Spectral line magnitude in dependence on TR.*

T_R [s]	Magnitude [-]
12	2.9
60	10
300	43.2
600	74.7
3060	142
300000	141.7

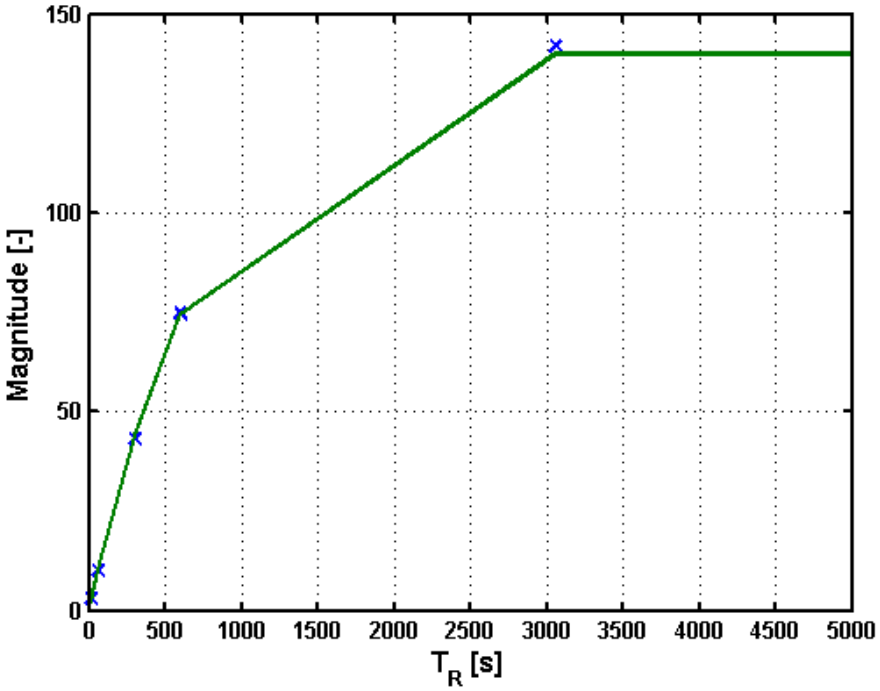

Fig. 22: *Spectral line magnitude dependence on repetition time T_R in saturation recovery experiment, for sample no. 7 – natural xenon under pressure at least 2 atm. The last measured value for T_R 300 000 sec is not shown because of a better and a more visible resolution for the shorter repetition times.*

6.1.2. Thermally polarized natural xenon in small samples

The next experiments were focused on determining the T_1 relaxation time. For these experiments two capsules were prepared, the first one with 2 bars of natural xenon with 26 mm in diameter, and the second one with 0.5 bar of oxygen (O_2) and 0.5 bar of xenon with 14.6 mm in diameter. Oxygen was used for T_1 relaxation time shortening.

The experiments were also based on the saturation recovery method. In the beginning of the experiment 10 (20 for sample with 2 atm of xenon) simple 90° presaturation pulses to break the thermal magnetization M_0 had been applied and then the measurement with settled repetition time T_R began. The spectral line magnitude is defined by saturation recovery equation

$$M = M_0\left(1-\exp\left(-\frac{T_R}{T_1}\right)\right), \tag{10}$$

where M is a signal magnitude in T_R, M_0 is a full magnitude of signal intensity, T_R is a repetition time, T_1 is a longitudinal relaxation time.

6.1.2.1. Sample filled in with 2 atm of xenon

The sizes of spectral lines for different T_R are shown in Tab. 5 and were fitted in Matlab (Fig. 23). The maximum size M = 10.7 of spectral line and T_1 relaxation time 2.2 hours were calculated.

Tab. 5: *Spectral line magnitude dependence on repetition times, saturation recovery*

T_R [hours]	Magnitude [-]
0	0
0.5	2.1
1	4
2.5	7.4
5	9.3
14	10.6
20	11

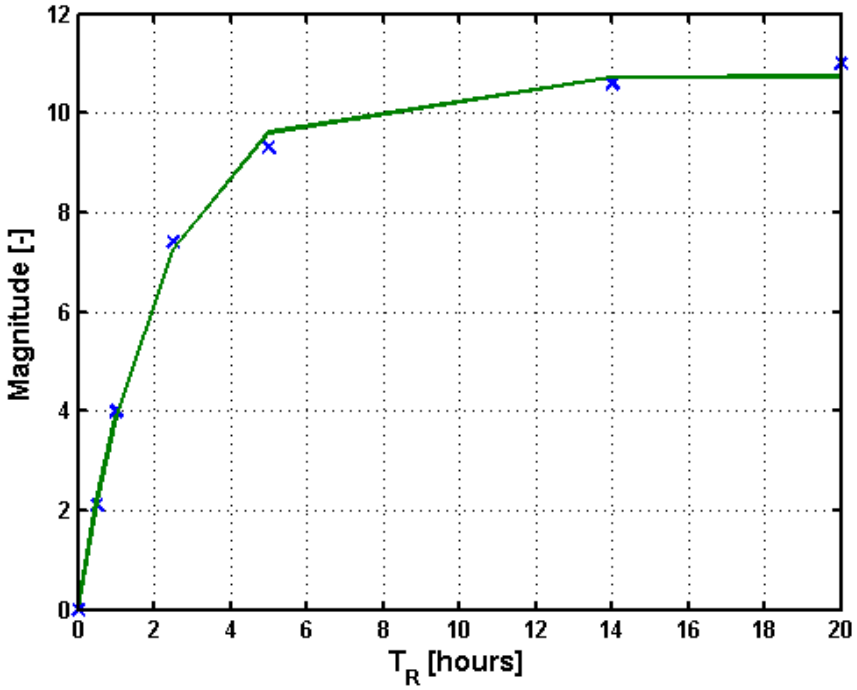

Fig. 23: *Spectral line magnitude dependence on repetition time T_R in saturation recovery experiment. Glass cell filled in with natural xenon 0.5 bar and oxygen 0.5 bar.*

6.1.2.2. Sample filled in with 0.5 atm of xenon and 0.5 atm of oxygen

The sizes of spectral lines for different T_R are shown in Tab. 6 and were also fitted in Matlab (Fig. 24). The maximum size M = 2.37 of spectral line and T_1 relaxation time 48.8 s were calculated.

Tab. 6: *Spectral line magnitude dependence on repetition times*

T_R [s]	Magnitude [-]
2	0
20	0.9
40	1.4
60	1.6
120	2.05
240	2.45

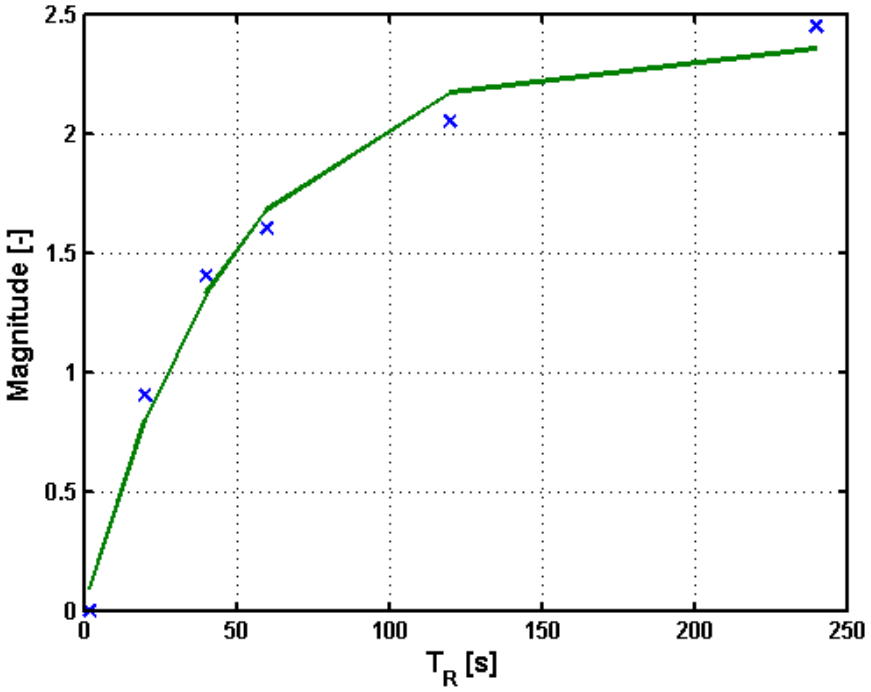

Fig. 24: *Spectral line magnitude dependence on repetition time T_R in saturation recovery experiment. Glass capsule filled in with natural xenon, 2 bars.*

6.1.3. Thermally polarized natural xenon in the „target cell“

For forthcoming experiments with hyperpolarized xenon new glass samples, which production is described in the chapter 5.1.2., were prepared. The first one was filled with a small amount of rubidium, xenon and nitrogen gas. The second one was filled with a small amount of rubidium and xenon gas. The absence of nitrogen gas allowed the rubidium vapour laser beam absorption to be visible to the naked eye. This enabled a better laser diode adjusting to the rubidium absorption line.

For the size of these samples new RF saddle coil was developed. It was 100 mm long and 40 mm in diameter. This larger coil was tuned in 54.767 MHz (synthesis frequency 54.267 MHz) and the sensitivity was around 4 times lower in comparison to a small saddle coil with 26 mm diameter.

Tab. 7: *Tab. X: Spectral line magnitude dependence on TR.*

T_R [min]	M [-]
0	0
10	0.28
15	0.8
30	1.0
45	1.15
70	1.1
3600	1.4

After 19 hours in 4.7 T magnetic field the first sample (Rb+N_2+Xe) was without any signal. Signal magnitudes of the second sample are shown in Tab. 7 and fitted in MATLAB (Fig. 25). The maximum magnitude of spectral line 1.31 and relaxation time T_1 22.67 min (1360.2 s) were enumerated.

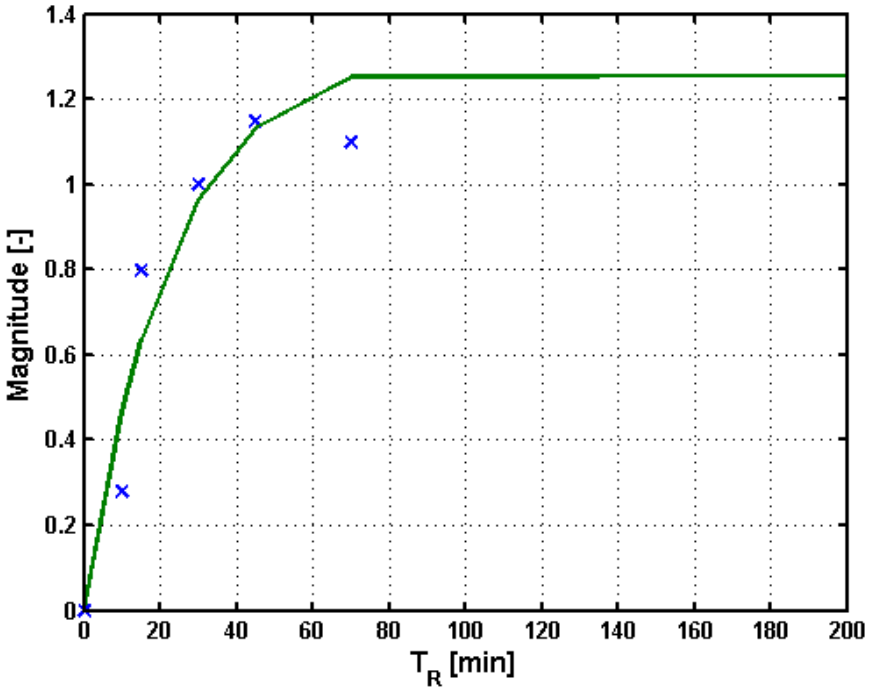

Fig. 25: *Spectral line magnitude dependence on T_R, after19 hours in 4.7 T. Glass sample filled with a piece of Rb and xenon. Thermally polarized. . The last measured value for T_R 3600s is not shown because of better and visible resolution for the shorter times*

Because of no signal from the sample with rubidium, xenon and nitrogen, a new cell was made. The cell (chapter 5.2.1) was filled with a small amount of rubidium, 1 atm of nitrogen, and 2 atm of xenon natural gas. This new sample was inserted in the magnetic field of 4.7 T for 47 hours (170000 s) to achieve the Boltzmann thermal equilibrium. After 47 hours the simple 90° pulse was applied and the spectral line magnitude was measured to be 24.3. The saturation recovery method was applied for data measurement (Tab. 8) and fitted in Matlab (Fig. 26). The T_1 relaxation time 1614 s (26.9 min) and spectral line maximum magnitude 24.1 was also enumerated in Matlab.

Tab. 8: *Spectral line magnitude in dependence on T_R*

T_R [s]	Magnitude [-]
0	0
600	9.4
1200	12.2
1800	15.2
3600	21.5
170000	24.3

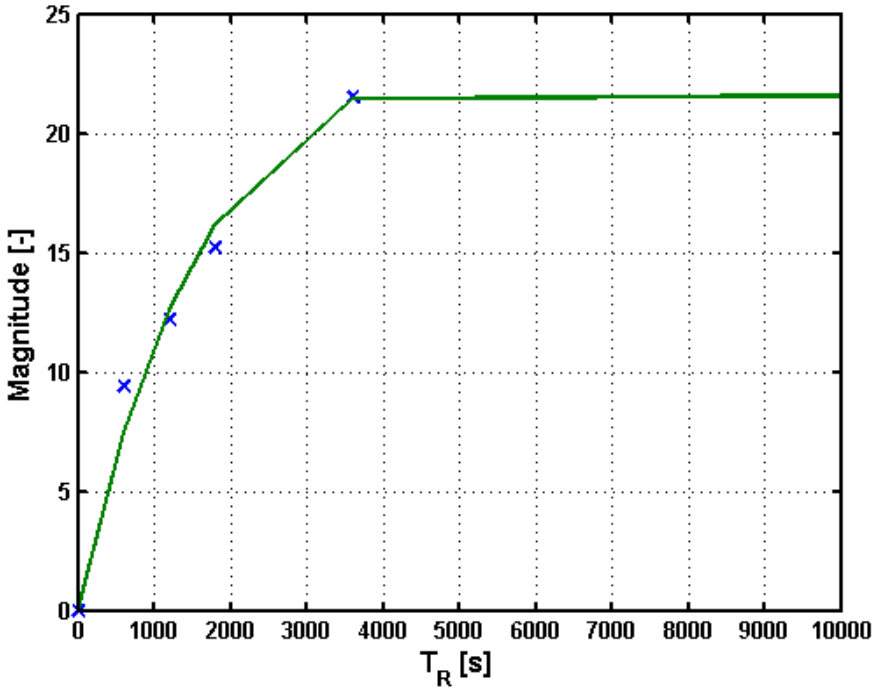

Fig. 26: *Spectral line magnitude in dependence on T_R. Thermally polarized xenon.*

6.2. Hyperpolarized xenon experiments

In comparison to experiments with thermally polarized xenon further experiments with hyperpolarized xenon were conducted. A cylindrical cell made from Simax glass was filled with natural xenon with natural abundance of ^{129}Xe. The cell was a simple 92 mm long cylinder with the diameter 35 mm. The cell's faces were made from Borofloat windows. On the cell's surface an Rb ampoule with a breakable glass valve was mounted. Before the cell was sealed, it had been filled under vacuum condition with a mixture of 100 kPa of xenon and 200 kPa of nitrogen. Than the breakable glass valve was broken and the ampoule was heated over rubidium melting point, which made it possible for the rubidium to be moved into the glass cell.

To allow thermostatization by a hot-air flow, the cell was enclosed in a teflon box. The box with the target cell was placed in front of the 4.7 T NMR system in homogenous 16 mT magnetic field.

A small amount of Rb was moved into the cell under vacuum conditions. Before the cell was sealed, it was filled with a mixture of xenon ^{129}Xe (100 kPa) and nitrogen N_2 (200 kPa). The target cell was heated to 100°C and the Rb vapour was optically pumped for 30 minutes. Then, the target cell was placed into the 4.7 T NMR system to obtain ^{129}Xe spectral line.

The spectral line of ^{129}Xe in natural state and the spectral line of the hyperpolarized ^{129}Xe are shown in Fig. 27. The amplification of the hyperpolarized xenon spectral line amplitude was about 400 times.

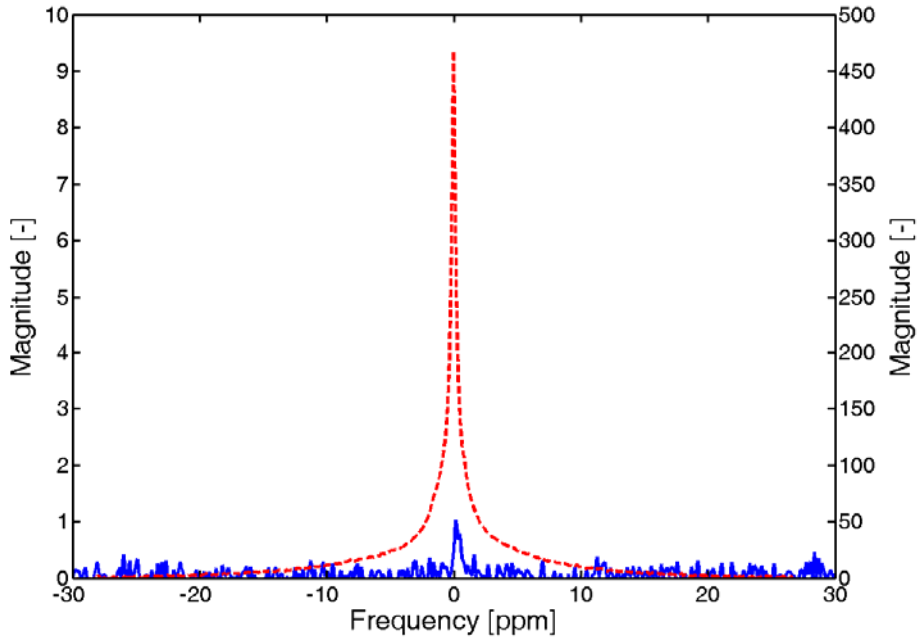

Fig. 27: *The thermally and hyperpolarized ^{129}Xe spectral line magnitude comparison.*

The influence of the optical pumping duration on the ^{129}Xe spectral line magnitude is shown in Fig. 28. Relaxation time T_1 is 26.9 minutes (1614 s) for natural state and 27.6 minutes (1656 s) for hyperpolarized state under given conditions.

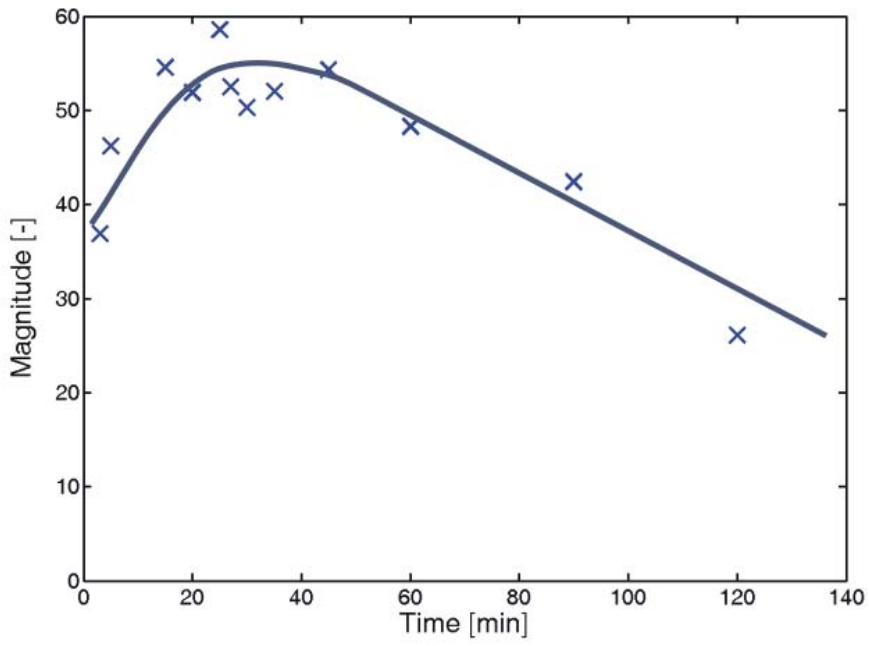

Fig. 28: *Dependence of magnitude of hyperpolarized xenon spectral line on duration of laser optical pumping.*

6.2.1. Hyperpolarized xenon inversion recovery experiment

The next experiment with hyperpolarized xenon was conducted using inversion recovery method.

The target cell containing mixture with nitrogen was inserted in the Teflon box. The hot air pistol was set to 130°C and the cell was being heated for 20 minutes. The laser beam emitted by laser diode in a free running mode was activated 10 minutes after the heating had begun. Thereafter, the cell was placed within 90 seconds in the 4.7 T NMR system. Ten presaturation pulses were applied and then the repetition time began. From T_R=10 min 20 presaturation pulses were applied.

Tab. 9: *Inversion recovery experiment with hyperpolarized xenon for T1 relaxation time calculation.*

T_R [min]	Magnitude [-]	FWHM [Hz]
3	0.9	27.1
5	1.3	32.9
10	1.3	37.7
20	1.8	29.6
50	2.8	28.7

The spectral lines magnitudes and their FWHM [Hz] (full width half maximum) are shown in Tab. 9. The T_R and magnitudes were fitted (Fig. 29) in Matlab. The maximum magnitude of 2.68 and T_1 relaxation time 12.86 min (771.6 s) were enumerated in Matlab as well.

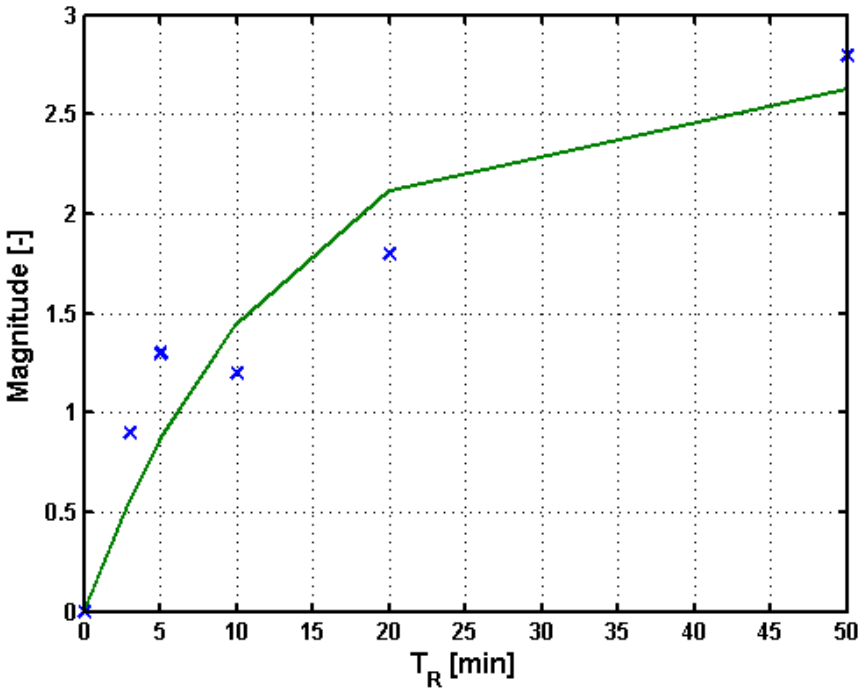

Fig. 29: *The dependence of hyperpolarized xenon magnitude on T_R fitted in Matlab.*

6.2.2. Hyperpolarized xenon relaxation in different magnetic field

The additional measurement concerned with hyperpolarized xenon relaxation in different magnetic field was conducted. For the experiment a glass cell with nitrogen was used. The glass cell was inserted in the Teflon box for better insulation and better warming up by a hot air pistol. The Teflon box was inserted into the Helmholtz coil generating 10 mT magnetic field. The hot air pistol was set to 130°C and the cell was heated for 20 minutes. After 10 minutes the laser beam emitted by laser diode in free running mode was activated. Thereafter the cell was placed in the 4.7 T NMR system within 90 sec. Then, after the repetition time T_R, simple 90° pulse was applied and the signal magnitude was measured. For the first experiment the target cell was inserted in 4.7 T magnetic field, while T_R was running. For the second and third experiment the cell was deposed on a chair in Earth's magnetic field respectively in the magnetic field generated by Helmholtz coil, while T_R was running. After T_R the experiment cell was inserted into the 4.7 T NMR system within 90 sec and simple 90° pulse was applied. The measured spectral lines magnitudes are shown in Tab. 10 and depicted in the Fig. 30.

Tab. 10: *The hyperpolarized xenon spectral line magnitude fall in different intensity of magnetic field and in the course of time.*

Measurement	t [min]	Magnitude [-]	FWHM [Hz]
in the 4.7 T magnetic field	5	55.4	28.2
	10	47.6	28.3
	20	27.6	29.7
	50	8.1	29.8
in the Earth's magnetic field	2	31.1	28.6
	5	7.8	28.4
	10	0.5	28.6
in 10 mT generated by Helmholtz coil	5	9	28
	10	1	29
	20	0.3	20

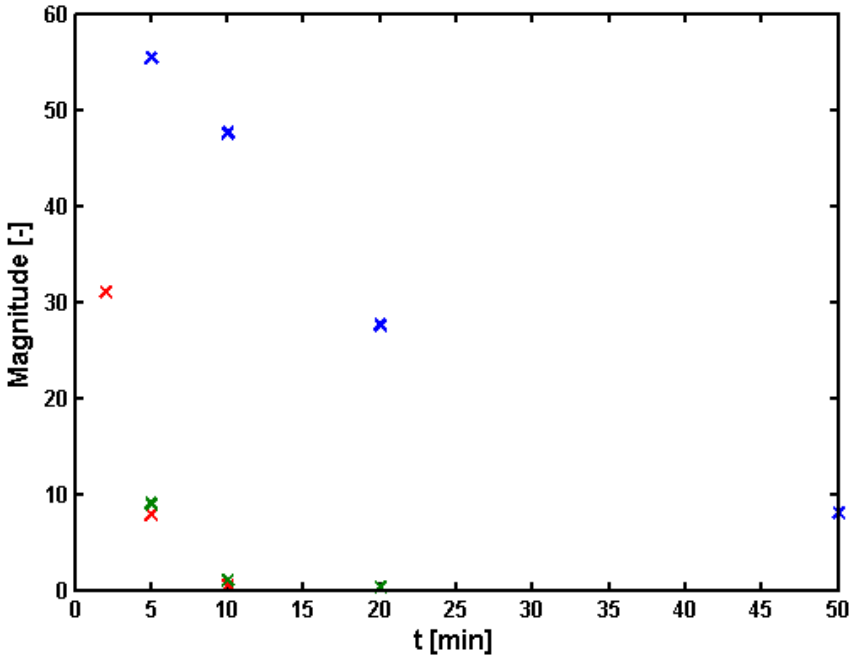

Fig. 30: *The dependence of hyperpolarized xenon spectral line magnitude on time. Target cell inserted for a time t in the 4.7 T magnetic field (blue), in the Earth's magnetic field (red) and in 10 mT generated by the Helmhotz coil (green).*

6.2.3. Xenon hyperpolarization by laser diode in broad or narrow mode and its spectral line magnitude

The last presented experiment shows the difference between xenon hyperpolarized by broad laser diode emission spectrum and narrow laser diode emission spectrum.

The high power laser diode was powered with 2.96 A and was tempered to 10.858°C.

The experiment had been conducted in a similar way to the previous one. The target cell containing the mixture with nitrogen was inserted into the Teflon box. The hot air pistol was set to 130°C and the cell was heated for 20 minutes. The laser diode emission spectrum in free running mode has been activated 10 minutes after the heating had begun. Thereafter, the cell was placed in the 4.7 T NMR system and simple 90° pulse was applied after the time period shown in Tab. 11.

Tab. 11: *The dependence of xenon spectral line magnitude on acquisition time after optical pumping in defined time t.*

	Narrow emission spectrum		Broad emission spectrum	
t [s]	Magnitude [-]	S/N [-]	Magnitude [-]	S/N [-]
40	698108	208.2	221019	67
40	583126	177.3	248583	76.2
40	596381	178.1	-	-
40	587946	178.8	-	-
60	528902	153.1	223386	68.7
60	535969	163.9	205959	63.8
60	532230	162.4	-	-
80	517564	156.6	-	-
80	478685	149.4	-	-
80	507712	154.9	-	-
120	449739	134.5	196006	59.9
120	462370	142.7	185345	56.9
160	392277	124.3	178974	55.7
160	404261	124.9	189439	58.2

The S/N (signal to noise) ratio was calculated as a magnitude (signal) divided by noise. The noise data are not shown Tab. 11 shown, but their value was around 3300.

Because of good measurement repeatability some magnitudes to be measured were skipped in the broad emission spectrum experiment.

In comparison to the previous hyperpolarized xenon experiments, which were conducted by the home-made electronic and control software, this experiment was conducted using the new electronic by MR Solution Ltd. That is why, the magnitudes seem to be much greater. However, by the comparison of S/N ratio, it has been shown that the data measured by the new system are comparable to the data obtained by the old system. The data are given in Fig. 31. There is also visible, the difference in magnitude of xenon hyperpolarization by broad (2.49 W) and narrow (1.49 W) emission spectrum.

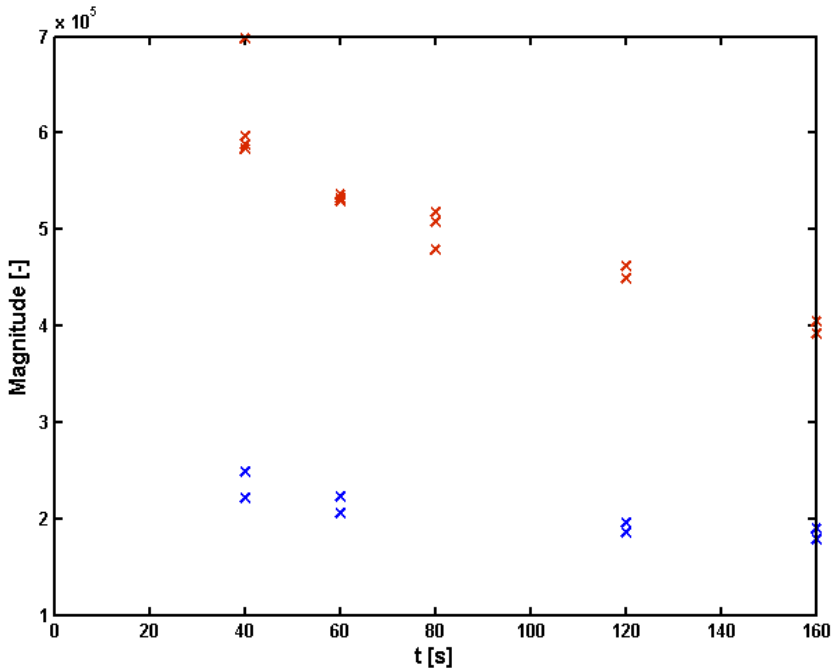

Fig. 31: *The time dependence of xenon hyperpolarization by broad and narrow emission spectrum. The time period represents duration of relaxation in 4.7 T NMR system after the laser was turned off.*

6.2.4. Preservation of magnetization

Experiments related to preservation of the hyperpolarized xenon magnetization were conducted in connection to the hyperpolarized xenon storage system concept. Experiments were conducted with the sample no. 1 described in subchapter 6.1.2.1.

a) After 10 hours in 4.7 T magnetic field the sample was taken out and placed into the Earth's magnetic field for 1 hour. After 1 hour it was put back to 4.7 T and 90° pulse was applied. The first attempt was without signal.

b) At the second attempt, the sample was in 4.7 T for the period of 10 hours. After that, it 90° pulse was applied. The spectral line size was 1.9. After the pulse was applied the sample was put in 4.7 T magnetic field for 30 minutes. Thereafter, the sample was taken out and placed into the Earth's magnetic field for 60 seconds. Then the sample was placed back into 4.7 T within 45 seconds. The 90° pulse was applied immediately after that and the xenon spectral line magnitude was 2.1.

c) The xenon spectral line magnitude time dependence was measured after the sample was taken out after being 30 minutes in 4.7 T to the Earth's magnetic field. The sample was in the Earth's magnetic field for defined time (Tab. 12) and then put back into the 4.7 T and 90° pulse was immediately applied. The Matlab approximation is in the Fig. 32. The fall to zero of the spectral line size is about 10 minutes.

Tab. 12: *Thermally polarized xenon spectral line magnitude in time dependence.*

t [min]	Magnitude [-]
0	2
1	2.7
2	2.15
3	2.2
5	1.6
8	1.2

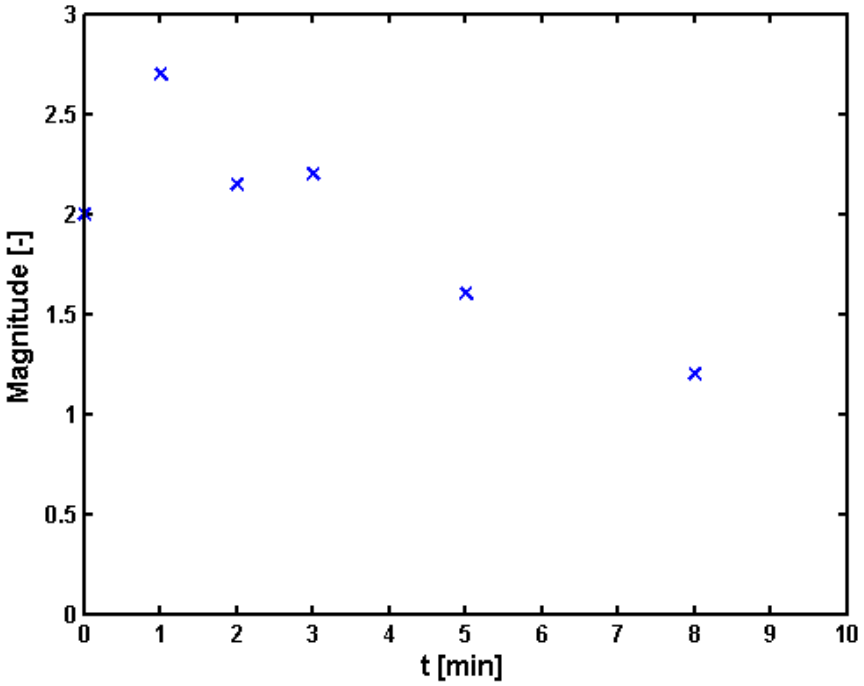

Fig. 32: *Thermally polarized xenon spectral line magnitude in dependence on time.*

d) Another experiment with liquid nitrogen was performed. After 10 hours in 4.7 T the sample was taken out and frozen to liquid nitrogen's temperature. After 1 hour the sample was removed from liquid nitrogen and put back in 4.7 T and 90° pulse was applied. The sample gave no xenon signal. The signal remain zero even during the next experiment when the sample was put for 30 minutes in 4.7 T and then for 5 minutes into Earth's magnetic field. Tab. 13 shows spectral line magnitudes of natural xenon after being for 30 minutes in 4.7 T and after being for defined time under liquid nitrogen temperature.

Tab. 13: *Spectral line size of natural xenon after 30 minutes in 4.7 T and after defined time t in liquid nitrogen. * - sample taken out before superconducting magnet (magnetic field of around 20 mT, ** - sample taken out before superconducting magnet and freezed to liquid nitrogen temperature, *** - sample taken out before superconducting magnet and insert to 16 mT magnetic field.*

t [min]	Magnitude [-]
0	2.1**
8	2.1**
15	1.4**
8	2.2*
8	1.6***

6.3. Continuous flow method

The previous experiments were conducted in a sealed cylindrical target cells made from borosilicate (Simax) glass.

The physical properties, predominantly T_1 relaxation time, of thermally polarized xenon, were measured by the "sealed" method. Many variation and measurement series were conducted. Some of them are presented in previous chapters. Measurement in the sealed regime was very time consuming, because after each scan the cell needed to be warmed up and optically pumped again. Or in case of thermally polarized xenon the Boltzmann equilibrium distribution had to be re-established.

In comparison to sealed regime, the continuous flow method allows continual spin-exchange optical pumping process in the target cell to be running in a magnetic field, sufficient for rubidium energy levels Zeeman splitting, outside of superconducting magnet (in e.g. Helmholtz coils or in stray field of superconducting magnet). With the aid of suitable tubing the target cell can be connected to a probe cell, which is placed in RF coil in MR system. Thus, the probe cell can be supplied by the new hyperpolarized gas in dependence to defined flow rate inside the system guaranteed by peristaltic pump.

In comparison with the aim specifications of the doctoral thesis, mentioned in chapter 2, the hyperpolarization under continuous flow was an extra task. With a continuous flow experimental device it would be easier to check the design of the xenon storage system, which is mentioned in chapter 6.3.2.

6.3.1. Continuous flow design

The continuous flow method design is depicted on scheme in Fig. 33. The scheme consists of three parts, the first is vacuum part based on turbomolecular drug pump described in subchapter 5.1.1., the second part is a gas delivery system, and the third part is the main part for the continual flow, consisting of Teflon tubing, O_2 and moisture filters, and flowmeter. The probe cell (Fig. 19) is a simple Simax cylinder connected with the Teflon tubing. Hyperpolarized xenon storage system and Foamglas box are depicted in Fig. 34.

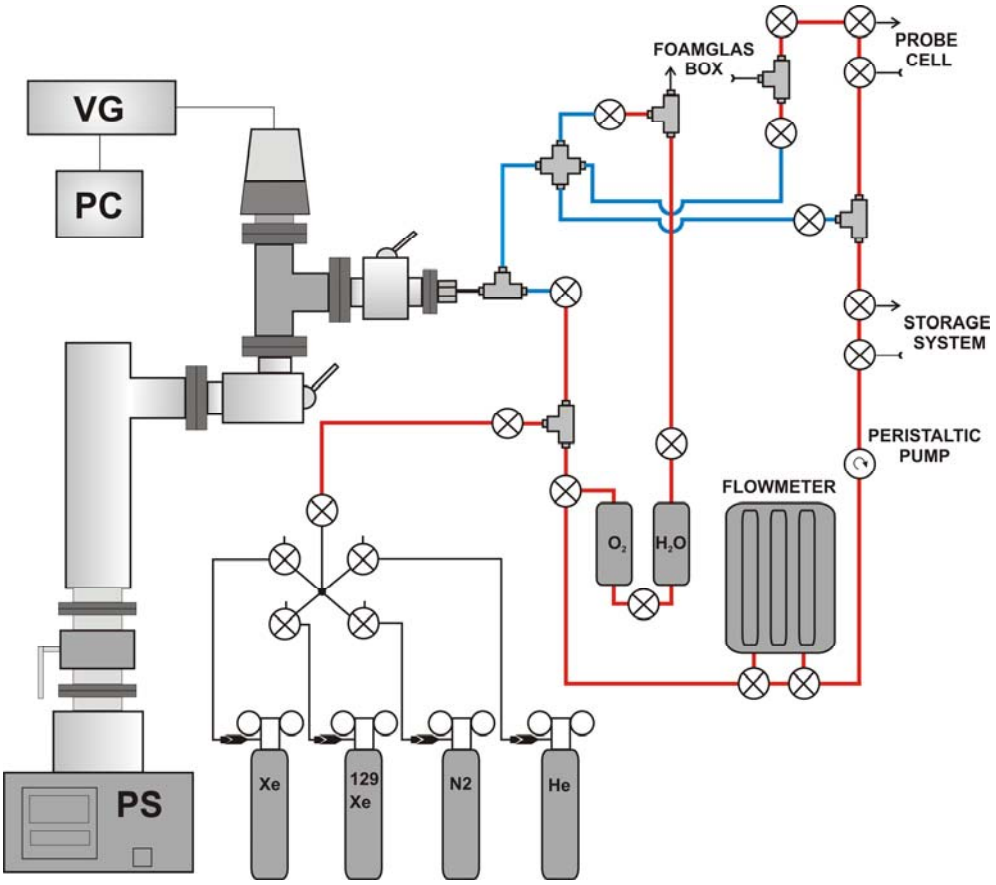

Fig. 33: *Continuous flow design. PS is turbomolecular drag pumping station, VG is vacuum valve, PC personal computer. Xe, ^{129}Xe, N_2 and He are gas bottles, O_2 and H_2O are oxygen respective moisture filters. The blue lines are connected to an evacuating system. The red lines are connected to a gas delivery system and make a closed circle for continual flow.*

The part labeled Foamglas box on the Fig. 34 and 35 is described in more detail in subchapter 5.1.3. The simplified schema is on the left hand side in Fig. 35. The storage system simplified schema is on the right hand side in Fig. 35 and described in more detail in subchapter 6.3.2.

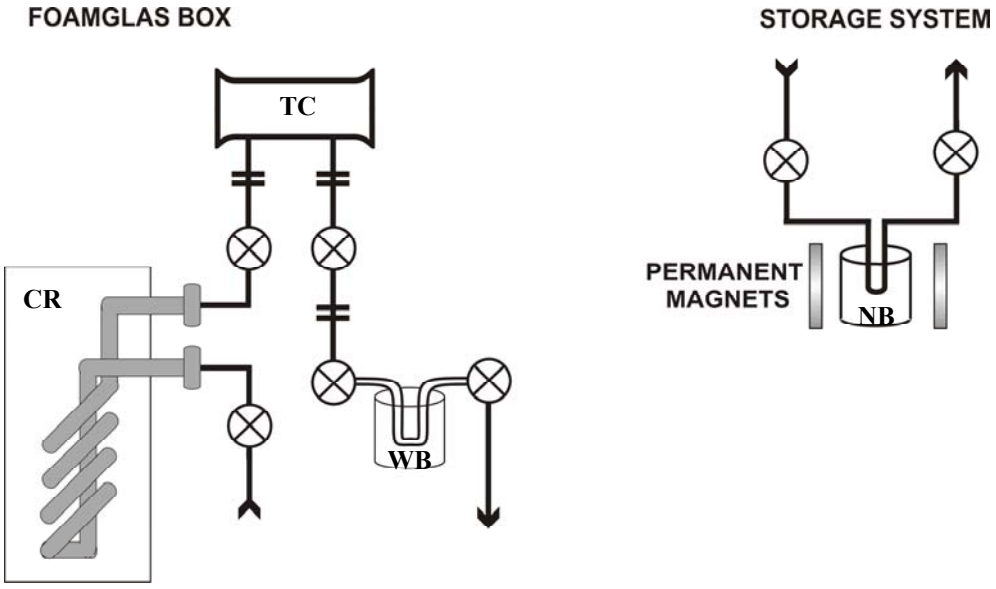

Fig. 34: *The scheme of Foamglas box contents and hyperpolarized xenon storage system. TC is the target cell, CR is chemical radiator, WB is the cold water bath, NB is the nitrogen bath (or nitrogen – alcohol mixture with the temperature of around -50°C).*

6.3.2. Hyperpolarized xenon storage system

In order to preserve the properties of HpXe, T_1 relaxation time especially, a simple xenon storage system had been suggested. It had been found [12, 43] that magnetic field, liquid nitrogen temperature, and non metallic parts can help to preserve the hyperpolarization of ^{129}Xe. The simplified schema of the storage system is depicted in the Fig. 34 and the real part in Fig. 36. The glass storage part, called “cold finger”, is in the middle of the permanent magnet, where the magnetic field is from 40 mT at the bottom, 60 mT in the middle, and 40 mT on the top – measured in the axis of the cold finger.

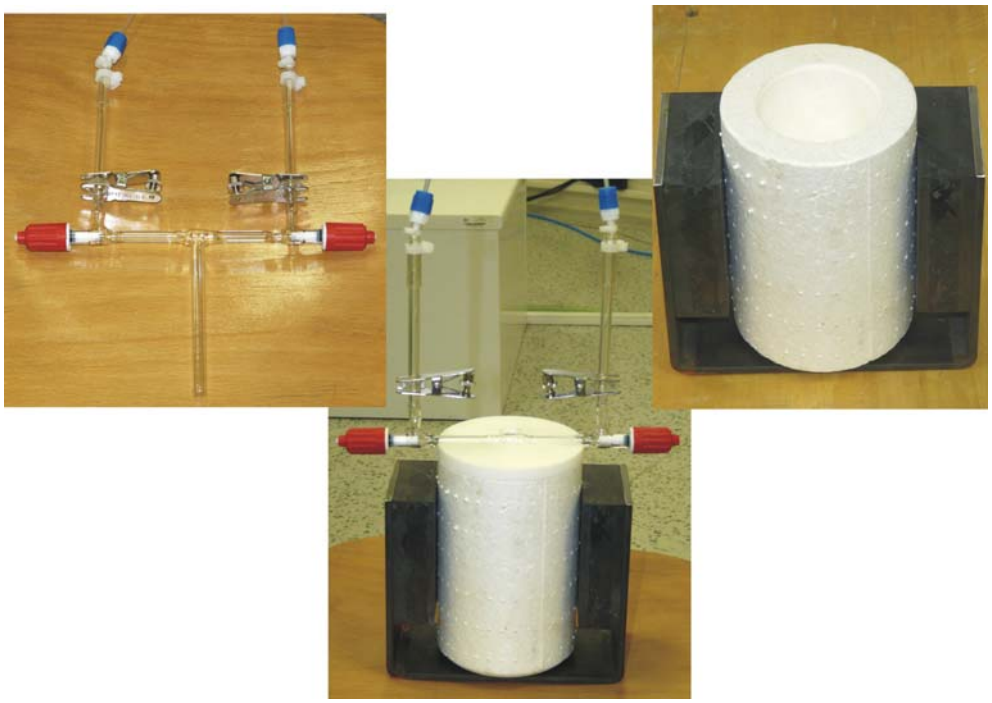

Fig. 35: *Storage system for frozen xenon.*

6.4. Impact of glass material on T_1 xenon relaxation time

The T_1 (longitudinal) relaxation time, known as a spin-lattice relaxation time is also influenced by the interaction of an investigated matter with a sample material. In our case the investigated matter is ^{129}Xe and sample material is Simax glass. In [42] is introduced a summary of how to reduce the wall relaxation time by coating cell's wall, and a washing procedure of the sample's inner wall.

In our case the target cells were washed with acetone and additional washing or coating procedures had not been executed. This chapter describes the experiment concerning xenon T_1 relaxation times influenced by the susceptibility of the glass cells.

For this experiment a cylindrical Delrin shell (Fig. 36) was prepared. The Delrin shell consisted of two parts, the first one is a main cylindrical body, in which the glass samples were inserted, and the second one is a screwed-on closure in which a Teflon stopcock by Torr Seal is affixed. The closure with body was sealed by a rubber ring.

Fig. 36: *Delrin shell with valve. On the right hand side are shown glasses samples.*

The glass samples were simple cylinders 100 mm in length and 26 mm in outer diameter. The four types of glasses were investigated: Simax, silica, Schott, and silica glass coated with Teflon.

A glass tube was inserted into the Delrin shell and the closed shell was filled with natural xenon pressurized to 3 atm. The electronics for experiment conduction were set on LB = 10 Hz, SI = 8k, SW = 20k, G1 = 20 dB, PW1 = 5 dB, p1 = 150 μs, f = 54.2691 MHz, NS = 1, PNS = 10.

The measured T_1 relaxation times and calculated values of the glass susceptibilities are shown in Tab. 14.

Tab. 14: *Xenon T_1 relaxation times and wall's susceptibility of used glasses*

	Simax	silica	Schott	silica + Teflon	Delrin
$\chi \cdot 10^{-6}$ [-]	-8.8	-8.79	-11.7	-8.79	-
T_1 [s]	1349	1025	1788	1459	1242

7. Conclusions

This dissertation thesis explores the development and construction of a 129Xe hyperpolarization device. Besides designing an experimental unit for HpXe production, this thesis also explores the noble gases theories, focusing on 129Xe and experimental verification of noble gases optical polarization efficiency in different physical conditions.

This dissertation may be divided in two primal parts: constructional and experimental.

The constructional part of this thesis covers not only a complex design of the 129Xe optical pumping hyperpolarization device, but also its implementation. Suggested device enables the production of HpXe in continuous flow regime. The basis for this device is a peristaltic pump that enables the gas mixture (Xe, He, N2) to flow in a defined rate through a target cell. The combination of a flow and pressure variability of xenon and buffer gases makes it possible to effectively research the polarization process efficiency in various physical conditions. Suggested system thus enables an examination of the influence of buffer gas pressures and a spectral magnitude of optical radiation on the HpXe production efficiency and in addition, an optimization of this process.

The constructional part of this thesis also includes a design and an implementation of a device for the HpXe transportation and storage.

The experimental part of this thesis compares thermal and optical polarization of xenon. At the beginning, trial experiments with thermally polarized xenon in order to confirm the ability of 4.7 T NMR system to detect xenon spectral line were conducted. These experiments were crucial for determination of optimal configuration and 4.7 T NMR system detection chain parameters.

After conducting the trial experiment and designing an RF coil, experiments with optical production of polarized xenon were initiated. Several sealed target cells were constructed and filled with mixtures of xenon, rubidium, and buffer gasses in various concentrations. These samples successfully confirmed the principle of optical hyperpolarization of xenon. These samples were also used to experimental determination of optimal time period for polarization of xenon with given capacity. At the same time, a direct link between power spectral density of a pumping beam and xenon polarization magnitude was established.

Furthermore, that experimental part of the dissertation was also interested in a study of relaxation time of xenon in diverse conditions. Established relaxation times fluctuated within the tens of seconds. This fact confirmed the necessity to design and construct a transportation case for the polarized gas that would prolong the period during which the gas is in a hyperpolarized state and therefore make it possible for the hyperpolarized gas to be used in medicine and material engineering.

The results of trial experiments with optically polarized xenon were subsequently applied in designing the previously mentioned experimental device for

production of polarized xenon in continuous flow regime. Based on the knowledge of working pressures and times that are necessary for reaching an optimal degree of polarization, a suggestion and a selection of individual components for the device for continual pumping was carried out. The components were selected in order to accommodate the requirements for securing the maximal effectiveness of polarization process in the continuous flow regime.

The evolution process of the device was concluded by series of successful pressure tests and a new set of experiments to explore the efficiency of continuous flow regime production is currently being planned.

8. References

[1] A. Kastler. Optical methods for studying hertzian resonances. Nobel Lecture, page 186, 1966.

[2] [online] http://en.wikipedia.org/wiki/Optical_pumping 12.9.2008

[3] M.R. Bouchiat, T.R. Carver, and C.M. Varnum. Nuclear polarization in he3 gas induced by optical pumping in dipolar exchange. Phys. Rev. Lett., 5(8):373-375, 1960.

[4] Happer, W. and Tam, A. C. *Effect of rapid spin exchange on the magnetic-resonance spectrum of alkali vapors,* Physical Review A, 1977, vol. 16, iss. 5, pp. 1877–1891

[5] Happer, W. *Optical Pumping*, Review Of Modern Physics, 1972, vol. 44, iss. 2, pp. 169–249

[6] Walker, T.G., Happer, W. Spin-exchange optical pumping of noble-gas nuclei, Rev. Mod. Phys. 1997, vol. 69, iss. 2, 629-642

[7] Rosen, M.S., Chupp, T.E., Coulter, K.P., Welsh, R.C.: Polarized ^{129}Xe optical pumping/spin exchange and delivery system for magnetic resonance spectroscopy and imaging studies, Rev. Sci. Instrum., 1999, vol. 70, iss. 2, pp.1546-1552

[8] Song, Y-Q, Goodson, B.M., Pines, A.: NMR and MRI using laser-polarized xenon, Spectroscopy, 1999, vol. 14, iss. 7, 26-33

[9] Tseng, C.H., Mair, R.W., Wong, G.P., Williamson, D., Cory, D.G., Walsworth, R.L.: Magnetic resonance imaging of laser polarized liquid xenon, Phys. Rev. E, 1999, vol. 59, iss. 2, 1785-1788

[10] Leawoods, J.C., Yablonskiy, D.A., Saam, B., Gierada, D.S., Conradi, M.S.: Hyperpolarized ^{3}He gas production and MR imaging of the lung, Concepts in Magn. Reson., 2001, vol. 13, iss. 5, pp. 277-293

[11] Brunner, E.: Enhancement of surface and biological magnetic resonance using laser-polarized noble gases, Concepts in Magn. Reson., 1999, vol. 11, iss. 5, pp. 313-335

[12] Duhamel, G.: Résonance magnétique nucléaire (RMN) in vivo du xénon-129 hyperpolarisé: Application à la mesure de la perfusion cérébrale chez le rat, 2001, PhD Thesis, Université Joseph Fourier, Grenoble

[13] Kilian, W.: Erzeugung von hyperpolarisiertem ^{129}Xe-Gas und Nachweis mittels in vivo NMR-Bildgebung, NMR-Spektroskopie sowie SQUID-Messtechnik, 2001, PhD Thesis, Freie Universität Berlin

[14] Wong, G.P., Tseng, C.H., Pomeroy, V.R., Mair, R.W., Hinton, D.P., Hoffmann, D., Stoner, R.E., Hersman, F.W., Cory, D.G., Walsworth, R.L.: A system for low field imaging of laser-polarized noble gas, J. Magn. Reson., 1999, vol. 141, pp. 217-227

[15] Tseng, C.H., Wong, G.P., Pomeroy, V.R., Mair, R.W., Hinton, D.P., Hoffmann, D., Stoner, R.E., Hersman, F.W., Cory, D.G., Walsworth, R.L.: Low-field MRI of laser polarized noble gas, Phys. Rev. Lett., 1998, vol. 81, is. 17, pp. 3785-3788

[16] Möller, H. E., Chawla, M. S., Chen, X. J., Driehuys, B., Hedlund, L. W., Wheeler, Ch. T., Johnson G. A.: *Magnetic resonance angiography with hyperpolarized ^{129}Xe dissolved in a lipid emulsion*, Magnetic Resonance in Medicine, 1999, vol. 41, no. 5, pp. 1058-1064

[17] Albert, M.S., Cates, G. D., Driehuys, B., Happer, W., Saam, B., Springer, C. S., and Wishnia, A.: *Biological magnetic-resonance-imaging using laser polarized 129Xe*, Nature, 1994, iss. 370, sp. 6486, pp. 199-201

[18] Saam, B., Yablonskiy, D. A., Gierada, D. S., and Conradi, M. S.: *Rapid imaging of hyperpolarized gas using EPI,* Mag. Rezon. Med., 1996, vol. 42, no. 3, pp. 507-514

[19] Driehuys, B., Moeller, H., Pollaro, J., and Hedlund, L.W. MR Imaging of Pulmonary Perfusion and Gas Exchange by Intravenous Injection of Hyperpolarized 129Xe. Proceedings of the 15th ISMRM: May 19-25, 2007, Berlin, Germany. ISSN 1545-4436].

[20] Chan, B., Nelson I. A., Anderson, L. W., Driehuys, B., and Walker, T. G. 129Xe-Xe molecular spin relaxation, Phys. Rev. Lett., vol. 88, Iss. 11, pp 113201, 2002.

[21] Driehuys, B., Cates, G. D., Miron, E., Sauer, K., Walter, D. K., and Happer, W., High-volume production of laser-polarized Xe-129, Applied Physics Letters, vol. 69, iss. 12, pp 1668-1670, 1996

[22] Driehuys, B., Alternate mechanisms for spin polarization. Proceedings of the 14th ISMRM: May 6-12, 2006, Florida, USA.]

[23] Cross, A., McPhee, D., Santyr, G.E., Wallace, J., Cheetham, J.J., Cron, G. Effects of Dilution and oxygenation on T1 of hyperpolarized 129Xe in perfluorocarbon emulsions. Proceedings of the 9th ISMRM: April 21-27, 2001, Glasgow, Scotland]

[24] Duhamel, G., Choquet, P., Grillon, E., Leviel, J.L., Ziegler, A., Constantinesco, A. Brain perfusion measurement using hzperpolarized xenon-129 MRI. Proceedings of the 10th ISMRM: May 18-24, 2002, Honolulu, Hawai.

[25] Venkatesh, A. K., Hong, K. S., Kubatina, L., Sun, Y., Mulkern, R., Jolesz, F. A., Albert, M. S.. Using dynamic hyperpolarized xenon MR to measure brain perfusion. Proceedings of the 9th ISMRM: April 21-27, 2001, Glasgow, Scotland]

[26] Dimitrov, I., Reddy, R., Leigh, J.S.: *Intermolecular dipole-dipole relaxation of ^{129}Xe dissolved in water*, J. Magn. Reson., 2000, vol. 145, pp. 302-306

[27] Goodson, B.M.: *Using injectable carriers of laser-polarized noble gases for enhancing NMR and MRI*, Concepts in Magn. Reson., 1999, vol. 11, is. 4, pp. 203-223

[28] Landon, C., Berthault, P., Vovelle, F., Desvaux, H.: *Magnetization transfer from laser-polarized xenon to protons located in the hydrophobic cavity of the wheat nonspecific lipid transfer protein*, Protein Science 10, 2001, pp. 762-770

[29] Song, Y-Q.: *Spin polarization induced nuclear Overhauser effect: An application of spin-polarized xenon and helium*, Concepts in Magn. Reson., 2000, vol. 12, iss. 1, pp. 6-20

[30] Locci, E., Dehouck, Y., Casu, M., Saba, G., Lai, A., Luhmer, M., Reisse, J., Bartik, K.: *Probing proteins in solution by ^{129}Xe spectroscopy*, J. Magn. Reson., 2001, vol. 150, pp. 167-174

[31] Bowers, C.R., Storhaug, V., Webster, C.E., Bharatam, J., Cottone, III A., Gianna, R., Betsey, K., Gaffney, B.J.: *Exploring surfaces and cavities in lipoxygenase and other proteins by hyperpolarized 129Xe NMR*, J. Am. Chem. Soc., 1999, vol. 121, pp. 9370-9377

[32] Luhmer, M., Goodson, B.M., Song, Y-Q., Laws, D.D., Kaiser, L., Cyrier, M.C., Pines, A.: *Study of xenon binding in cryptophane-A using laser-induced NMR polarization enhancement*, J. Am. Chem. Soc., 1999, vol. 121, pp. 3502-3512

[33] Rubin, S.M., Spence, M.M., Pines, A., Wemmer, D.E.: *Characterization of the effects of nonspecific xenon-protein interactions on ^{129}Xe chemical shifts in aqueous solution: Further development of xenon as a biomolecular probe*, J. Magn. Reson., 2001, vol. 152, pp. 79-86

[34] Mair, R.W., Hurlimann, M.D., Sen, P.N., Schwartz, L.M., Patz, S., Walsworth, R.L.: *Tortuosity measurement and the effects of finite pulse widths on xenon gas diffusion NMR studies of porous media*, Magn. Reson. Imaging, 2001, vol. 19, pp. 345-351

[35] Moudrakovski, I.L., Lang, S., Ratcliffe, C.I., Simard,, B., Santyr, G., Ripmeester, J.A.: *Chemical shift imaging with continuously flowing hyperpolarized xenon for the characterization of materials*, J. Magn. Reson., 2000, vol. 144, pp. 372-377

[36] Jameson, C.J., Jameson, A.K., Kostikin, P., Baello, B.I.: *Adsorption of xenon and CH_4 mixtures in zeolite NaA. ^{129}Xe NMR and grand canonical Monte Carlo simulations*, J. Chem. Phys., 2000, vol. 112, no. 1, pp. 323-334

[37] Springuel-Huet, M-A., Bonardet, J-L., Gédéon, A., Fraissard, J.: *^{129}Xe NMR overview of xenon physisorbed in porous solids*, Magn. Reson. Chem., 1999, vol. 37, pp. 1-13

[38] Wang, R.: *Study of gas flow dynamics in porous and granular media with laser-polarized ^{129}Xe NMR*, PhD. Thesis, 2005, Massachusetts institute of technology, Cambridge

[39] J. Becker. Study of mechanical compression of spin-polarized 3he gas. Nucl. Instrum. Methods Phys. Res. A, 346(1-2):45{51, 1994.

[40] J. Becker, J. Bermuth, M. Ebert, T. Grossmann, W. Heil, D. Hofmann, H. Humblot, M. Leduc, E.W. Otten, D. Rohe, and R. Surkau. Interdisciplinary experiments with polarized 3he. Nucl. Instrum. Methods Phys. Res. A, 402(2-3):327{336, 1998.

[41] T.R. Gentile, G.L. Jones, A.K. Thompson, R.R. Rizi, D.A. Roberts, I.E. Dimitrov, R. Reddy, D.A. Lipson, W. Gefter, M.D. Schanll, and J.S. Leigh. Demonstration of a compact compressor for application of metastability-exchange optical pumping of 3he to human lung imaging. Mag. Res. Med., 43(2):290{294, 2000.

[42] Buchta, Z., Rychnovský, J., Lazar, Lazar, J.: *Optical pumping of Rb by Ti:Sa laser and high-power LD,* Journal of Optoelectronics and Advanced Materials, 2006, vol. 1, pp. 350 – 354, ISSN 1454-4164

[43] Mansson, S.: Hyperpolarized Nuclei for NMR Imaging and Spectroscopy. PhD. Thesis, 2002, University of Lund, Sweden. ISBN 91-628-5434-8

[44] Ruset, C. I.: *Hyperpolarized ^{129}Xe production and applications*, PhD. Thesis, 2005, University of New Hampshire, Durham

[45] Morris, P. G.: Nuclear magnetic resonance imaging in medicine and biology. Oxford University Press, New York, 1986. 388 pages. ISBN 0-19-855155-X

[46] Wang, H-T. J.: New *xenon gas polarizer with application to magnetic resonance imaging*, PhD. Thesis, 2007, University of Virginia, Charlottesville

[47] Frossati, G.: Polarization of ^3He, D_2 (and possibly ^{129}Xe) using cryogenic techniques. Nucl. Instrum. Meth. A 1998; 402:479–483.

[48] Bouchiat, M.A., Carver, T.R., Varnum, C.M.: Nuclear polarization in He^3 gas induced by optical pumping and dipolar exchange. *Phys Rev Lett* 1960; 5:373–375.

[49] Kastler, A.: Quelques suggestions concernant la production optique et la détection optique d'une inégalité de population des niveaux de quantification spatiale des atomes: application ŕ l'expérience de Stern et Gerlach et ŕ la résonance magnétique. J. Phys. Rad. 1950; 11:255–265.

[50] Grover, B.C.: Noble-gas NMR detection through noble-gas-rubidium hyperfine contact interaction. Phys. Rev. Lett. 1978; 40:391–392.

[51] Alkali D Line Data. 2009. http://steck.us/alkalidata/

[52] Bifone, A.: Production of optically polarized xenon for medical applications. In: Maraviglia B, ed. Magnetic resonance and brain function: approaches from physics. IOS Press, Amsterdam 1999. p. 493–503.

[53] Happer, W.: Optical pumping. Rev. Mod. Phys. 1972; 44:169–249.

[54] Franken, P.A., Colegrove, F.D.: Alignment of metastable helium atoms by unpolarized resonance radiation. Phys. Rev. Lett. 1958; 1:316–318.

[55] Colegrove, F.D., Franken, P.A.: Optical pumping of helium in the $^3S_1$ metastable state. Phys Rev 1960; 119:680–690.

[56] Colegrove, F.D., Schearer, L.D., Walters, G.K.: Polarization of He^3 gas by optical pumping. Phys Rev 1963; 132:2561–2572.

[57] Gamblin, R.L., Carver, T.R.: Polarization and relaxation processes in He^3 gas. Phys Rev 1965; 138:A946–A960.

[58] Daniels, J.M., Shearer, L.D., Leduc, M., Nacher, P.J.: Polarizing ^3He nuclei with neodymium $La_{1-x}Nd_xMgAl_{l1}O_{19}$ lasers. J. Opt. Soc. Am.1987; B4:1133–1135.

[59] Driehuys, B., Cates, G.D., Miron, E., Sauer, K., Walter, D.K., Happer, W.: High-volume production of laser-polarized 129Xe. Appl Phys Lett 1996; 69:1668–1670.

[60] Goodson, B.M.: Nuclear magnetic resonance of laser-polarized noble gases in molecules, materials, and organisms. J Magn Reson 2002; 155:157–216.

[61] Saturatin recovery. 2009. http://www.mritutor.org/mritutor/satrecov.htm

[62] R.L. de Zafra. Optical pumping. *Am. J. Phys.*, 28:646-654, 1960.

[63] R. Benumof. Optical pumping theory and experiments. *Am. J. Phys.*, 33:151-160, 1965.

[64] T.J. Killian. Thermionic phenomena caused by vapors of rubidium and potassium. *Phys. Rev.*, 27(5):578-587, 1936.

[65] M.E. Wagshul and T.E. Chupp. Laser optical pumping of high-density rb in polarized 3he targets. Phys. Rev. A, 49(5):3854-3869, 1994.

[66] S. Appelt, A. Ben-Amar Barange, C.J. Erickson, M.V. Romalis, A.R. Young, and W. Happer. Theory of spin-exchange optical pumping of 3he and 129xe. Phys. Rev. A, 58(2):105-108, 1998.

[67] H. E. Moller, X. J. Chen, B. Saam, K. D. Hagspiel, G. A. Johnson, T. A. Altes, E. E. de Lange, and H. U. Kauczor. MRI of the lungs using hyperpolarized noble gases. *Magn Reson Med*, 47(6):1029{51, 2002.

[68] G. Peach: Theory of the pressure broadening and shift of spectral-lines, Advances in Physics,vol. 30, pp. 367-474 (1981)

[69] W. F. Meggers, C. H. Corliss and B. F. Seribner, Tables of spectral-line intensities, Part I (1961)

[70] Z. Buchta, J. Rychnovský, J. Lazar: Optical pumping of Rb by Ti:Sa laser and high-power LD, Journal of materials science: Materials in electronics, Iss. 1, vol. 8, pp. 350-354 (2006)

[71] M. Vrbová et al., Lasery a moderní optika, Oborová encyklopedie, ISBN 80-85849-56-9 (1994)

[72] http://www.rp-photonics.com/semiconductor_lasers.html

[73] A. S. Arnold, J. S. Wilson and M. G. Boshier: A simple extended-cavity diode laser, Rev. Sci. Instrum., vol. 69, pp. 1236-1239 (1998)

[74] K. Liu and M. G. Littman: Novel geometry for single-mode scanning of tunable lasers, Opt. Lett., vol. 6, 1980, pp. 117-118 (1980)

[75] P. McNicholl and H. J. Metcalf: Synchronous cavity mode and feedback wavelength scaning in dye laser oscillators with grating, Appl. Opt., vol. 24, pp. 2757-2761 (1985)

[76] Buchta Z, Číp O and Lazar J, High-power extended cavity laser optimized for optical pumping of Rb, Measurement Science and Technology, vol. 18, pp. N77-N80 (2007)

[77] http://www.home.agilent.com/agilent/product.jspx?pn=6654a